

Bio-inspired step-climbing in a hexapod robot

Ya-Cheng Chou, Wei-Shun Yu, Ke-Jung Huang and Pei-Chun Lin

Department of Mechanical Engineering, National Taiwan University, Taipei, Taiwan

E-mail: peichunlin@ntu.edu.tw

Received 15 August 2011


Accepted for publication 13 March 2012

Published 1 May 2012

Online at stacks.iop.org/BB/7/036008

Abstract

Inspired by the observation that the cockroach changes from a tripod gait to a different gait for climbing high steps, we report on the design and implementation of a novel, fully autonomous step-climbing maneuver, which enables a RHex-style hexapod robot to reliably climb a step up to 230% higher than the length of its leg. Similar to the climbing strategy most used by cockroaches, the proposed maneuver is composed of two stages. The first stage is the ‘rearing stage,’ inclining the body so the front side of the body is raised and it is easier for the front legs to catch the top of the step, followed by the ‘rising stage,’ maneuvering the body’s center of mass to the top of the step. Two infrared range sensors are installed on the front of the robot to detect the presence of the step and its orientation relative to the robot’s heading, so that the robot can perform automatic gait transition, from walking to step-climbing, as well as correct its initial tilt approaching posture. An inclinometer is utilized to measure body inclination and to compute step height, thus enabling the robot to adjust its gait automatically, in real time, and to climb steps of different heights and depths successfully. The algorithm is applicable for the robot to climb various rectangular obstacles, including a narrow bar, a bar and a step (i.e. a bar of infinite width). The performance of the algorithm is evaluated experimentally, and the comparison of climbing strategies and climbing behaviors in biological and robotic systems is discussed.

 Online supplementary data available from stacks.iop.org/BB/7/036008/mmedia

(Some figures may appear in colour only in the online journal)

1. Introduction

Compared to wheeled vehicles, whose advantage lies in smooth and power-efficient mobility on flat ground, legged systems are excellent at negotiating uneven terrain. Generally speaking, locomotion generation involves three cycling steps: sense, think and act. Research of wheeled robots typically focuses on the sensing and algorithm, but not on the act, because of their straightforward motion-generation mechanism. In contrast, research of legged robots focuses on their mobility in uneven environments, where the integration of sensing, strategy and coordination of leg locomotion is crucial. Among all these studies, step-climbing is one of the associated topics of research.

Locomotion of aerial, ground and underwater animals is the source of bio-inspired robots (Plamondon and Nahon 2009,

Jusufi *et al* 2010, Low and Chong 2010); the cockroach is one of the important ground animals that is widely studied, and it serves as a source of imitation. The cockroach (*Blaberus discoidalis*) adjusts its body posture to climb over obstacles (Watson *et al* 2002a, 2002b) or stairs (Shaoping *et al* 2000). Its musculoskeletal structure can stabilize rapid locomotion on challenging terrains by using neural (Sponberg and Full 2008) and/or distributed mechanical feedback (Spagna *et al* 2007); this feedback mechanism helps the cockroach to maintain its equilibrium and resist disturbances (Dickinson *et al* 2000). In addition, cockroaches use visual means and antennae to guide their actions, such as running along walls (*Periplaneta americana*) (Cowan *et al* 2006, Camhi and Johnson 1999), knowing the position of an object (*P. americana*) (Okada and Toh 2000) and managing different climbing or passing strategies (*B. discoidalis*) (Harley *et al*

2009). Besides cockroaches, lizards (*Sceloporus malachiticus*) also use different strategies to cross obstacles of different heights (Kohlsdorf and Biewener 2006, Kohlsdorf and Navas 2007). In short, with a feedback mechanism and adequate motion strategy, the cockroach performs rapid and robust locomotion on uneven terrain, and serves as the source of our bio-inspired work.

On the robotic side, various studies related to robots climbing obstacles have been reported, with most results evaluated while the robots were using their ordinary walking gaits. For example, the MechaRoach uses four-bar mechanisms as legs, and it can climb over 70% of its standing height (Bogges *et al* 2004). The Sprawlita can climb obstacles that are belly-high (Cham *et al* 2004), and its successor, iSprawl, which has a similar capability, has a faster running speed and is power-autonomous (Kim *et al* 2006). The Whegs I can overcome an obstacle 1.5 times as high as the radius of its leg-wheel hybrids (Quinn *et al* 2003). When it encounters tall barriers, its compliant front legs can passively adapt themselves to climb the barrier in coordination, while the designed leg phases basically remain unchanged. The Whegs II has an extra dorsal DOF and antenna. When it senses the barrier, the dorsal DOF is bent to lift the front body up, and it can climb over obstacles twice as high as the radius of its leg-wheel hybrids (Lewinger *et al* 2005). Its successor, DAGSI Whieg, has an actively controlled and passively compliant body joint, and it can climb steps 2.19 times the length of its leg-wheel hybrids (Boxerbaum *et al* 2008). The RHex, the original style of the platform used in this work, demonstrates great mobility on various uneven terrains via simple open-loop control, due to its simple and robust morphology (Saranli *et al* 2001). By using a pre-defined tripod walking gait, it can surmount obstacles 80% of the length of its leg, at a speed of one body length per second, and pass over rough surfaces of random heights, with a maximum variation of 116% of the length of its leg. It can run on wire mesh, where 90% of the surface is removed (Spagna *et al* 2007). With leg sensors and an inertia measurement unit, the body state of the RHex, with open-loop dynamic jogging gaits, can be correctly measured (Lin *et al* 2005, 2006). With enhanced sensory feedback, the RHex can also run on a rough brick terrain (Weingarten *et al* 2004). It can climb stairs with its four-bar legs (Moore and Buehler 2001) and half-circle legs (Moore *et al* 2002), and it can gradually transition its gait from normal tripod walking to the stair-climbing gait developed by Moore *et al* (Clark Haynes and Rizzi 2006). The robot's first-step motion of stair-climbing is, to a certain degree, similar to that of the step-climbing maneuver. The first-step algorithm for stair-climbing developed by Moore *et al* requires one of the robot's front legs to catch the stair and pull the robot onto the first step; this motion is basically similar to that of a robot approaching a step using the tripod gait. However, when the step is too high for the front leg to catch, this strategy is not feasible, and the failure mode of the robot to climb high steps with either the tripod or stair-climbing gait is the same. Thus, for the RHex to climb high steps, it is necessary to find other approaches. The quadruped LittleDog, with three DOFs per leg, uses dedicated leg trajectories to climb steps via optimization and learning

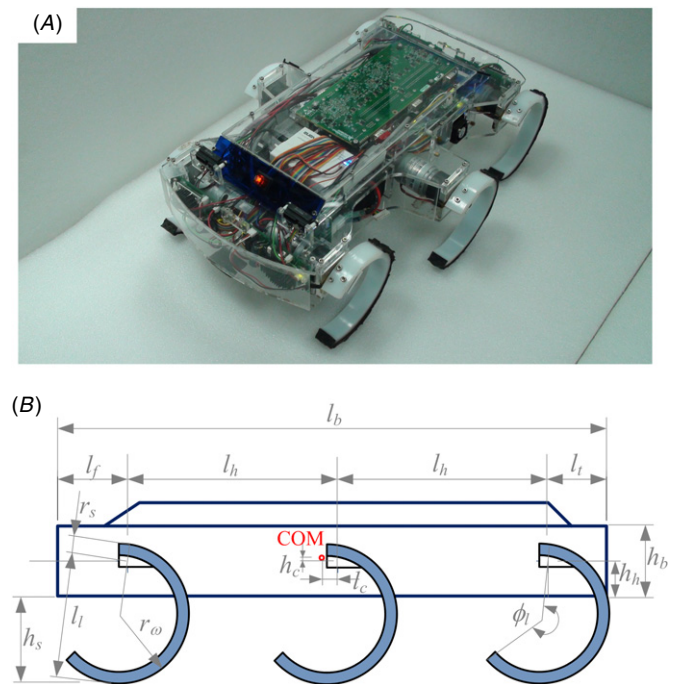


Figure 1. Robot information: (A) photo of the RHex-style hexapod robot for experimental evaluation; (B) symbols of the robot's dimensions. The physical dimensions are listed in table 1.

(Zucker *et al* 2011, Kalakrishnan *et al* 2011); however, this method is not effective for the RHex, as it has only one DOF per leg. In addition, without a dorsal DOF, the approach adopted by the Whieg series is not feasible, either. To summarize, many reported works address the mobility issues of the original walking gait when a robot faces obstacles, and some address special maneuvers for step-climbing. However, none of them is applicable for the RHex-style robot, and investigating a new approach is desired.

The maneuver used by cockroaches when they encounter high obstacles inspired us to develop a new gait for the RHex-style robot, shown in figure 1, to climb a step with a height of no less than its body height. The literature reveals that $\sim 70\%$ of the time, the cockroach climbs high obstacles in two stages: the 'rearing stage', which changes the body inclination before any leg reaches the obstacle, and the 'rising stage', which lifts the center of mass (COM) with little or no further change in body inclination. Hereafter, this method is referred to as the 'rearing/rising strategy' (Watson *et al* 2002b). An illustrative sketch of the step-climbing locomotion of the cockroach is depicted on the right side of figure 2. This climbing strategy was adopted as the guideline for the development of the step-climbing maneuver in the hexapod robot. Here, based on our initial trials (Chou *et al* 2011), the goal of this archival-level work is (i) to find the right bio-inspired maneuver of the robot's COM to climb steps by coordinating the motions of its legs and (ii) to search for a simple feedback mechanism so the robot can reliably and automatically climb steps with a wide, but accessible, range of heights. More specifically, by targeting 'autonomous step-climbing', the robot should be capable of (i) sensing the step in front of it, (ii) detecting the height of

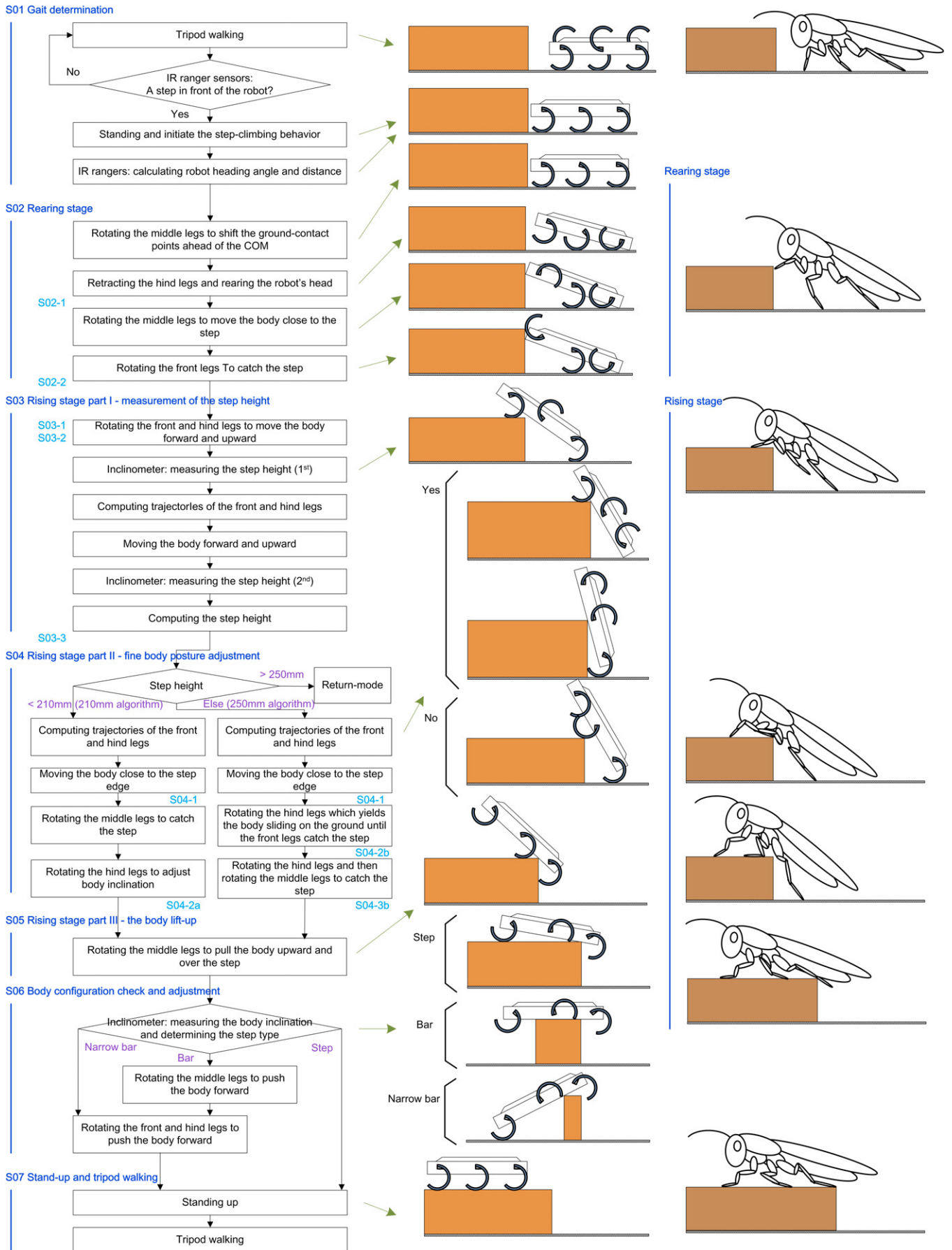


Figure 2. Flow chart of the overall algorithm and corresponding configurations of the robot and the cockroach.

the step, (iii) automatically generating the adequate maneuver and (iv) reliably performing the step-climbing maneuver. To the best of our knowledge, this work presents: (i) a unique bio-inspired maneuver designed specifically for step-climbing that utilizes only leg maneuvers and is significantly different from the normal walking gait; and (ii) automatic gait-changing and fine gait adjustment so the robot can successfully climb a wide range of high steps (up to 230% of its leg length) that it cannot negotiate using other developed gaits.

Section 2 describes in detail the design of the bio-inspired step-climbing maneuver, based on kinematic analysis. With an understanding of our approach, section 3 discusses the intrinsic properties and differences of the gaits performed in the biological system and in the robot under current development. Section 4 reports the results of the evaluation of the experiment, and section 5 concludes the work.

2. Design of the step-climbing maneuver

Legged locomotion, in general, is generated by the sequential or simultaneous propulsion of individual legs to the body in a time sequence. Thus, while the obstacle negotiation capability of the robot is judged by the success of the robot COM maneuver, it is, in principle, determined by how the legs interact with the ground and transmit the adequate propulsion force to maneuver the main body. The interaction of the leg with the ground is determined by the leg morphology and motion of the leg. For each kind of obstacle with a particular shape, there exists a certain leg morphology that is favored for negotiating this specific obstacle. However, for developing a general-purpose robot where the leg morphology is usually determined, the obstacle negotiation capability of the robot is mainly determined by the gait design.

The normal walking gait in the biological and robotic systems can negotiate rough terrain to a certain degree, as the periodic leg motion in general contains an aerial phase where the leg often lifts and swings. For example, the cockroach can climb a 5.5 mm high step with a normal tripod gait, and it uses different gaits to climb higher steps (Watson *et al* 2002b). The RHex-style hexapod robot uses continuous rotation of its legs to generate the ground and aerial phases (i.e. Buehler clock (Saranli *et al* 2001)), so the robot has very large ground clearance in the normal tripod walking gait, which helps in negotiating obstacles. Therefore, the first task in developing the step-climbing maneuver was to statistically evaluate how high a step the robot could climb with its normal tripod-walking gait.

Empirical evaluation shows that the RHex-style robot (figure 1(A)) utilizing a normal tripod walking gait and operating at a forward speed of 145 mm s^{-1} can adequately climb a step height up to 150 mm with a 100% success rate. Although the robot can also climb a 170 mm high step with 100% success and 180 mm with a 40% success rate, the robot body often collides with the ground and the step during climbing. In addition, because the tripod gait of the robot generates asymmetric propulsion force, the heading of the robot is usually badly altered after the robot climbs up

Table 1. Robot dimensions.

Length (mm)	Height (mm)	Leg (mm)
l_b 470	h_b 60	l_l 107
l_t 55	h_h 25	r_ω 65
l_h 178	h_s 82	r_s 22
l_f 60	h_c 7	
l_c 13		ϕ_l 240°

Table 2. Robot variables.

d_f	Robot heading distance
θ	Robot heading angle
α	Body pitch angle
ϕ_f, ϕ_m, ϕ_h	Orientation of front leg, middle leg and hind leg, respectively
X_{fh}, Z_{fh}	Coordinates of the front hip
X_{mh}, Z_{mh}	Coordinates of the middle hip
X_{hh}, Z_{hh}	Coordinates of the hind hip
h	Measured step height

onto the step. Moreover, the robot will fall from the side edges if the step is not wide enough. As a result, the 150 mm step height was treated as the upper limit the robot could pass with a correct heading while operating in the normal tripod-walking gait. Different gaits are required for the robot to climb steps higher than 150 mm.

The fundamental rule for the robot when climbing a step is to successfully maneuver the COM up onto the step, as the biological systems do. The effective first action to achieve this goal is to place the front legs on top of the step and then to lift the robot COM, using leg motion. When the step is too high for the front leg to reach, the robot should incline the body to raise the height of the front hips so the front legs can access the top of the step (i.e. ‘rearing stage’). After that, COM shifting can be executed in the ‘rising stage’. The overview of the developed motion sequence is depicted in the middle column of figure 2, and the detailed quantitative analysis is described in the following paragraphs in this section. Please note that the first paragraph in each motion task (i.e. S01, S02, ...) describes the motion design in a qualitative manner, and the remaining paragraphs in the same motion task quantitatively formulate the motion. Various symbols are utilized, as shown in figure 1(B) and table 2. For consistency and clear representation, the robot body in the associated figures is depicted in different colors, based on the motion tasks.

S01: Initiation of the step-climbing maneuver. When the robot uses the normal tripod gait, it simultaneously senses the environment in front of it. When a step is observed in its path, the robot stops walking and changes its gait to standing, preparing for initiation of the step-climbing behavior in motion task S02.

Two infrared (IR) range sensors were installed on the front of the robot to check for the presence of the step and the robot’s configuration relative to it. As shown in figure 3(A), two parameters are utilized to define the relative configuration: heading angle, θ , and heading distance, d_f , which are defined

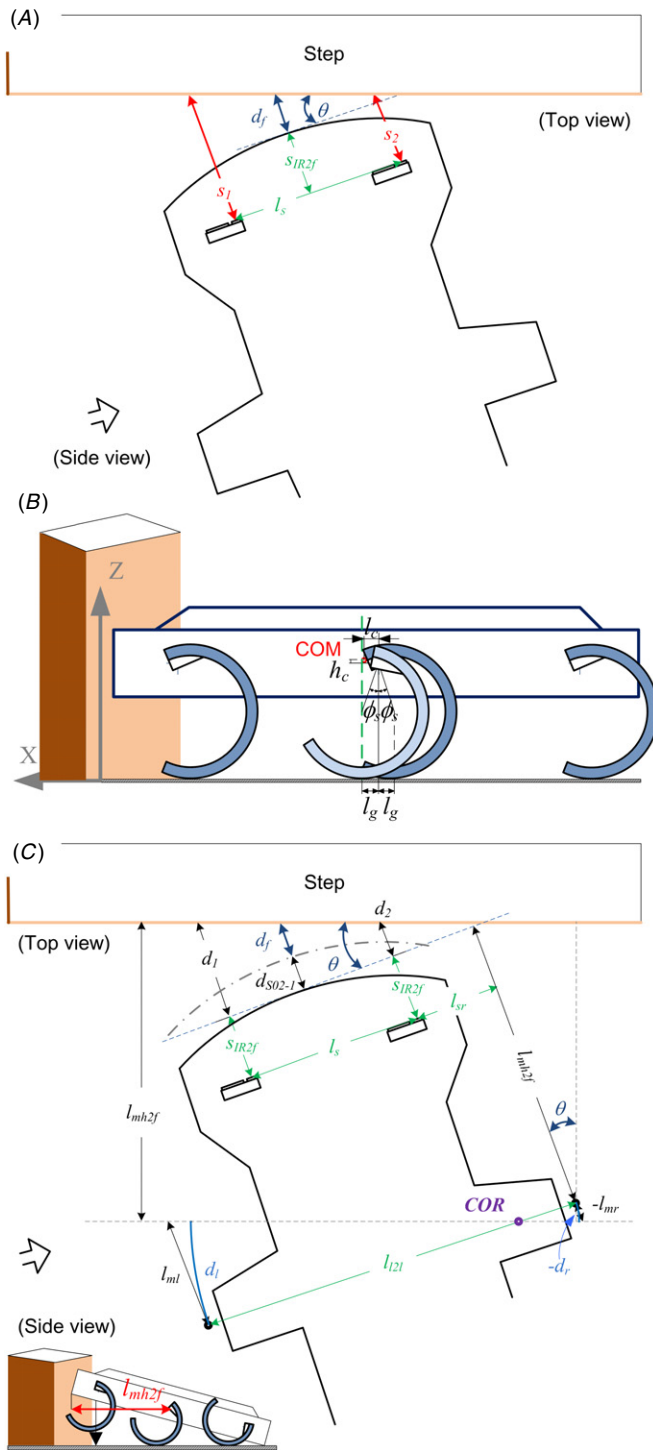


Figure 3. Robot configurations and terminologies associated with motion tasks S01 and S02, rearing stage. (A) Top view and (B) side view of the robot when it stands in front of the wall of the step in motion task S01. (B) Two possible leg configurations when the robot poses in the standing posture. Normal leg orientations are depicted in dark blue. (C) Configuration of the robot after body inclination in S02-1. The gray dashed line represents the original position of the front of the body before body inclination. The dimensions in this figure are the horizontal projections of the original dimensions (i.e. top view).

as the angle between the heading of the robot and the step and the shortest distance from the robot to the step, respectively. Assuming that the distance measurements of the sensors are

s_1 and s_2 , respectively, the heading distance and heading angle can be derived as

$$\theta = \tan^{-1} \left(\frac{s_1 - s_2}{l_s} \right) \quad (1)$$

$$d_f = \frac{s_1 + s_2 - 2s_{IR2f}}{2},$$

where l_s is the distance between the sensors and s_{IR2f} is the distance between the sensor and the front of the body, as shown in figure 3(A). During tripod walking, two states shown in (1) are computed in real time. If the robot approaches the step at a very shallow angle (i.e. large heading angle), the robot continues walking and turns to avoid the step, which does not initiate the step-climbing maneuver. The step-climbing maneuver is triggered when at least one of s_1 and s_2 , as well as the heading angle, are below certain thresholds. After the trigger, the robot switches its tripod walking to the standing posture. The final configuration of the standing robot relative to the step varies, due to different heading angles and standing times; figure 3(A) depicts the general relative configuration. This configuration is measured once more by the IR range sensors to compute the states shown in (1), which are utilized for further posture compensation in the following S02 rearing stage.

The accelerometer was utilized as the simple sensing mechanism in our initial trials (Chou *et al* 2011). When the robot bumped into the step, great forward deceleration was detected, and the step-climbing maneuver was initiated. However, because the detected impact could not reveal the robot's orientation relative to the step, the step-climbing was successful only when the robot walked directly toward the step. Moreover, when the robot encountered low steps, where the normal tripod walking gait could be utilized to climb the step, the robot still initiated the climbing maneuver, even though it was not necessary, because of the impact. The revised mechanism reported in this paper is generalized and suitable for general scenarios, where the robot may walk toward the step at different heading angles. The IR range sensors are installed around 148 mm above the ground, so that the step-climbing maneuver does not activate when the robot encounters low obstacles. In addition, the relative configuration can be correctly estimated, as shown in (1). Together with the posture compensation described in the next motion task, S02, the robot can climb the step from a wider range of orientation with respect to the step.

S02: Rearing stage. Motion task S02 has two purposes: first, to raise the front as high and as close to the edge of the step as possible, so the front legs can easily catch the top of the step in the next motion, task S03. The second purpose is to correct the various initial standing configurations of the robot to a unified body posture in preparation for climbing. To achieve these goals, the leg maneuver strategy is designed as follows. (i) The robot rotates the middle legs to shift their ground-contact points forward; thus, the COM of the robot's body is located between the middle and hind legs. (ii) The robot retracts the hind legs; gravity causes the body to incline, raising the front. (iii) The robot rotates the middle legs to move the body forward, until the front of the body touches the wall of the step. If the robot faces the step at a non-zero heading

angle, the right and left middle legs rotate at different rates to correct the body posture.

The quantitative analysis of S02 is detailed as follows. The contact point between the robot leg and the ground in the normal robot standing posture is located behind the hip, due to the setting of the positive shift angle, ϕ_s , as shown in figure 3(B). The dimensions of the robot have an intrinsic property

$$l_g = (r_\omega - r_s) \sin(\phi_s) > l_c, \quad (2)$$

where l_c is the horizontal distance of the COM to the middle hip, l_g is the horizontal distance of the middle leg ground contact point to the middle hip, and r_ω and r_s are the leg parameters, as shown in figure 1(B). With a middle leg orientation setting of $\phi_m = -\phi_s$, the ground contact point of the middle leg can be shifted to the other feasible location ahead of the COM without altering the standing height, as depicted in figure 3(B). Thus, after the retraction of the hind legs, the robot pitches backward (i.e. clockwise, negative value), as shown in figure 3(C). The body state in this configuration is hereafter referred to as S02-1.¹ The body pitch angle α is a function of ϕ_m , and can be represented as

$$\alpha_{S02-1} = f_\alpha(\phi_m) = -\tan^{-1}\left(\frac{r_\omega}{l_3}\right) - \tan^{-1}\left(\frac{l_2}{l_1}\right), \quad (3)$$

with

$$\begin{aligned} l_1 &= l_h + l_t + (r_\omega - r_s) \sin(-\phi_m) \\ l_2 &= (r_\omega - r_s) \cos(-\phi_m) - h_h \\ l_3 &= \sqrt{l_1^2 + l_2^2 - r_\omega^2}, \end{aligned} \quad (4)$$

where l_h , l_t and h_h are dimensions of the robot shown in figure 1(B) and l_1 , l_2 and l_3 are derived dimensions shown in figure 4. After body inclination, the body front moves backward, in a horizontal direction, at distance d_{S02-1} , as shown in figure 3(C):

$$\begin{aligned} d_{S02-1} &= (l_f + l_h) - l_{mh2f} \\ &- (r_\omega - r_s) \sin(-\phi_m) \\ &- (r_\omega - r_s) \sin(\phi_m + \alpha_{S02-1}) - r_\omega \alpha_{S02-1}, \end{aligned} \quad (5)$$

with

$$\begin{aligned} l_{mh2f} &= l_4 \cos\left(-\alpha_{S02-1} - \sin^{-1}\left(\frac{h_h}{l_4}\right)\right) \\ l_4 &= \sqrt{(l_h + l_f)^2 + h_h^2}, \end{aligned} \quad (6)$$

where l_f is the distance between the front of the body to the front of the hips, as shown in figure 1(B), l_{mh2f} is the distance between the middle hips to the front of the body, as shown in figure 3(C), and l_4 is a derived dimension, shown in figure 4. Equation (5) calculates the results of change in distance from body inclination, shown in the first line, and leg rolling, shown in the second line.

¹ Note that the overall step-crossing behavior is composed of several different motion tasks in sequence, which may be based on different mathematical formulas. To simplify the mathematical representation to be readable, the formulas describing current motion are formulated in the form of ‘incremental change,’ starting from the beginning of the particular motion task, where the initial conditions (i.e., the final state of the ‘previous’ motion task) are presumably known. The frequently used body states are body pitch angle α , leg orientations, and hip coordinates $(X_i, Z_i)_{i=fh, mh, hh}$, where fh , mh , and hh represent the front, middle, and hind hips, respectively.

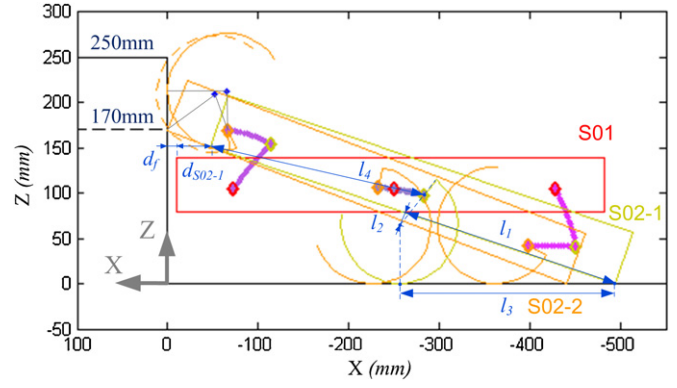


Figure 4. S02, rearing stage: maneuver of the body configuration in motion task S02: from initial condition S01 (red color), to S02-1 (yellow color), where the body is pitched backward, to S02-2 (orange color), where the body is moved forward. The diamond shapes represent the hip positions in the S01, S02-1, and S02-2 configurations. The line segments in purple, light purple and magenta indicate the trajectories of the front, middle and hind hips, respectively, in the overall S02 motion. The orange legs indicate the final leg configuration in S02-2.

Next, the middle legs rotate to move the body toward the step, until the body front lightly touches the wall of the step; this configuration is hereafter referred to as S02-2. Figure 3(C) depicts the notations for the quantitative computation associated with this motion. Generally, when the heading angle θ is non-zero, the two middle legs rotate at different rates to correct the body posture until it is perpendicular to the step (i.e. $\theta = 0$). During the correction, the body pitch angle and heights of the middle hips with respect to the ground change slightly due to leg rolling; however, these two small variations are ignored to simplify the kinematic computation. In the S02-2 configuration, the distance between the wall and the middle legs is basically equal to l_{mh2f} , shown in (5), where both dimensions are depicted in figure 3(C). The figure shows that if the robot can be rotated with respect to the center of rotation (COR) in the horizontal plane, the robot can configure in the S02-2 configuration. To achieve this goal, the right- and left-middle hip trajectories in the horizontal plane should move according to d_r and d_l :

$$\begin{aligned} d_r &= (l_{mr} \cot \theta) \theta \\ d_l &= (l_{l2l} + l_{mr} \cot \theta) \theta, \end{aligned} \quad (7)$$

with

$$\begin{aligned} l_{mr} &= l_{mh2f} - (l_{mh2f} \sec \theta - (d_2(l_{sr} + l_s) - d_1 l_{sr}) / l_s) \\ d_i &= s_i - s_{IR2f} + d_{S02-1}, \end{aligned} \quad (8)$$

where l_{l2l} and l_{sr} are the dimensions of the robot, as shown in figures 3(C). If the heading angle θ computed in (1) is zero, equation (7) reveals that both d_r and d_l are equal to l_{mr} . In addition, because in this scenario d_1 and d_2 are equal as well, equation (8) yields

$$l_{mr} = d_1 = d_2 = d_f + d_{S02-1}, \quad (9)$$

where the parameters are depicted in figure 3(C). With derived d_r and d_b , shown in (7), the amounts of middle leg motions $\Delta\phi_{mr}$ and $\Delta\phi_{ml}$ can be derived by the leg-rolling equations

$$\begin{aligned} d_j &= (r_\omega - r_s) (\sin(\phi_{mS02-1} + \Delta\phi_{mj} + \alpha_{S02-1}) \\ &- \sin(\phi_{mS02-1} + \alpha_{S02-1})) + r_\omega \Delta\phi_{mj=r,l}. \end{aligned} \quad (10)$$

As a result, the tilted body posture (i.e. non-zero heading angle) can be corrected with the compensated $\Delta\phi_{mr}$ and $\Delta\phi_{ml}$ executed in robot motion tasks S02-1 to S02-2.

Following the computation described above, the state of the robot in the S02-2 configuration can be quantitatively formulated thoroughly, including the final body pitch angle α_{S02-2} and the coordinates of the front and hind hips represented as the functions of α_{S02-2} :

$$\begin{aligned} (X_{fh}, Z_{fh})_{S02-2} &= \begin{bmatrix} -l_f \cos(-\alpha_{S02-2}) - h_h \sin(-\alpha_{S02-2}) \\ (l_b - l_f) \sin(-\alpha_{S02-2}) + h_h \cos(-\alpha_{S02-2}) \end{bmatrix}^T \\ (X_{hh}, Z_{hh})_{S02-2} &= \begin{bmatrix} -(l_b - l_t) \cos(-\alpha_{S02-2}) - h_h \sin(-\alpha_{S02-2}) \\ l_t \sin(-\alpha_{S02-2}) + h_h \cos(-\alpha_{S02-2}) \end{bmatrix}^T \end{aligned} \quad (11)$$

where l_b is the dimension of the robot shown in figure 1(B). The front and hind legs contact the ground and the step with leg orientations

$$\begin{aligned} \phi_f &= -\pi + \sin^{-1} \left(\frac{-r_\omega - X_{fhS02-2}}{r_\omega - r_s} \right) - \alpha_{S02-2} \\ \phi_h &= -\frac{\pi}{2} - \sin^{-1} \left(\frac{r_\omega - Z_{hhS02-2}}{r_\omega - r_s} \right) - \alpha_{S02-2}, \end{aligned} \quad (12)$$

respectively. Figure 4 depicts the body maneuver and hip trajectories in the overall S02 motion, from the initial condition S01, to S02-1, to ‘rearing posture’ S02-2. The final leg configurations are plotted in orange.

If the step height h is less than

$$Z_{fhS02-2} - (r_\omega - r_s) \cos(\phi_f + \alpha_{S02-2}) = 210.5 \text{ mm} \quad (13)$$

but higher than the 150 mm initiation height of the step-climbing behavior, the robot front still touches the wall of the step (i.e. α_{S02-2} the same) at the final configuration. However, instead of touching the wall of the step, the front leg catches the edge of the step, as shown in figure 4 in dashed orange curves (referred to as S02-2b). Front leg orientation ϕ_f can be solved by the following geometrical constraint:

$$\begin{aligned} &[-X_{fhS02-2} + (r_\omega - r_s) \sin(\phi_{fS02-2b} + \alpha_{S02-2})]^2 \\ &+ [Z_{fhS02-2} - (r_\omega - r_s) \cos(\phi_{fS02-2b} + \alpha_{S02-2}) - h]^2 = r_\omega^2. \end{aligned} \quad (14)$$

In this case, front leg orientation ϕ_f is a function of step height h .

In practical implementation, the leg trajectories are generated based on the described kinematic analysis. For the leg maneuver whose trajectories are fixed and not adjusted in real time (i.e. from S01 to S02-1), the leg trajectory can be pre-computed and coded in the onboard computer. In contrast, the maneuver from S02-1 to S02-2 not only pushes the body forward, but also corrects various initial body standing configurations in S01 to a unified posture based on the sensory feedback from the IR range sensors. In this case, the computation of the described kinematic equations or their approximations needs to be programmed onboard and computed in real time.

S03: Rising stage part I—measurement of the step height.

The robot has a rigid body without any spine DOF, so the initial body posture before step-climbing determines whether the following leg motions can effectively propel the body

upward or not. Moreover, because the step height strongly determines the adequate body posture for step-climbing, it should be correctly estimated in the early stage of the step-climbing behavior. The step height, h , can be measured while the robot is configured in the posture with the front and hind legs standing on the top and bottom of the step with the formula

$$\begin{aligned} h &= (r_\omega - r_s) \cos(\phi_h + \alpha_{\text{step}}) + 2l_h \sin(-\alpha_{\text{step}}) \\ &\quad - (r_\omega - r_s) \cos(\phi_f + \alpha_{\text{step}}), \end{aligned} \quad (15)$$

where α_{step} is the body pitch angle as shown in figure 5(A). To achieve this ‘measurement posture’ from the S02-2 posture shown in figure 4(B) (in orange), the robot first rotates the front legs to roll up the wall of the step, then it rotates both the front and hind legs to move the body forward and upward, until the front legs have grasped the top of the step. The necessity of this two-step action mainly results from geometrical constraints, which will be discussed in detail in the following paragraph.

The quantitative analysis of S03 is detailed as follows. Assuming that no geometry conflict exists, and pure rolling motion of the front legs up the wall of the step is feasible, the trajectories of the front hips can be represented as

$$\begin{aligned} (X_{fh}, Z_{fh}) &= \begin{bmatrix} -r_\omega + (r_\omega - r_s) \sin(\phi_{fS02-2} + \alpha_{S02-2} + \Delta\phi_f + \Delta\alpha) \\ Z_{fhS02-2} - (r_\omega - r_s) \cos(\phi_{fS02-2} + \alpha_{S02-2}) \\ + r_\omega (\Delta\phi_f + \Delta\alpha) \\ + (r_\omega - r_s) \cos(\phi_{fS02-2} + \alpha_{S02-2} + \Delta\phi_f + \Delta\alpha) \end{bmatrix}^T. \end{aligned} \quad (16)$$

Similarly, the rolling of the hind leg on the ground can be computed as

$$\begin{aligned} (X_{hh}, Z_{hh}) &= \begin{bmatrix} X_{hhS02-2} - (r_\omega - r_s) \sin(\phi_{hS02-2} + \alpha_{S02-2}) \\ + r_\omega (\Delta\phi_h + \Delta\alpha) \\ + (r_\omega - r_s) \sin(\phi_{hS02-2} + \alpha_{S02-2} + \Delta\phi_h + \Delta\alpha) \\ r_\omega + (r_\omega - r_s) \cos(\phi_{hS02-2} + \alpha_{S02-2} + \Delta\phi_h + \Delta\alpha) \end{bmatrix}^T. \end{aligned} \quad (17)$$

Based on (16) and (17), the instantaneous motion directions of the front and hind hips with the rolling motion can be derived as

$$\begin{aligned} (dX_{fh}, dZ_{fh}) &= \begin{bmatrix} (r_\omega - r_s) \cos(\phi_{fS02-2} + \alpha_{S02-2} + \Delta\phi_f + \Delta\alpha) \\ r_\omega - (r_\omega - r_s) \sin(\phi_{fS02-2} + \alpha_{S02-2} + \Delta\phi_f + \Delta\alpha) \end{bmatrix}^T \end{aligned} \quad (18)$$

and

$$\begin{aligned} (dX_{hh}, dZ_{hh}) &= \begin{bmatrix} r_\omega + (r_\omega - r_s) \cos(\phi_{hS02-2} + \alpha_{S02-2} + \Delta\phi_h + \Delta\alpha) \\ -(r_\omega - r_s) \sin(\phi_{hS02-2} + \alpha_{S02-2} + \Delta\phi_h + \Delta\alpha) \end{bmatrix}^T. \end{aligned} \quad (19)$$

In reality, the computed instantaneous COR of the robot body in the S02-2 configuration, with front and hind legs in a rolling motion, is located at the orange square mark shown in figure 5(B). Thus, the robot cannot move, as the four-leg-rolling motion moves the body, pushing it into the wall of

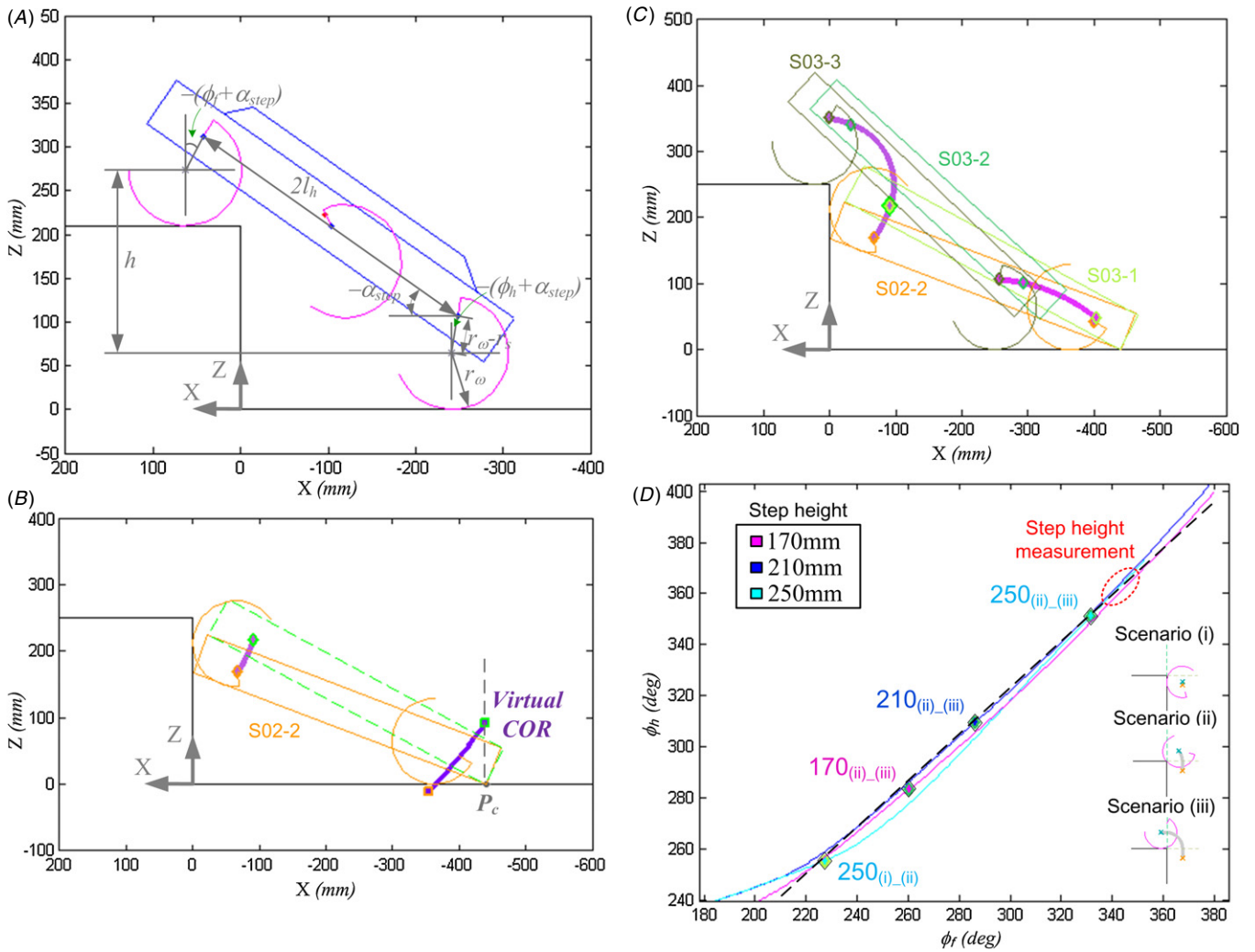


Figure 5. S03, rising stage part I—measurement of the step height: (A) ‘measurement posture,’ at which the height of the step can be detected from robot body inclination information. (B) Trajectories of the front hip (purple curve) and the ‘virtual’ COR of the robot with four-leg-rolling motion (dark purple) during the rolling-up motion of the front legs (i.e. ‘first action’). The configuration of the body (in dashed bright green) indicates the earliest moment of four-leg rolling motion (i.e. ‘second action’). (C) The combination of the first and second actions comprise motion task S03, which moves the robot body from the initial S02-2 configuration to measurement posture S03-3. The position of the front hips at the time of switching from the first action to the second action is marked by a bright green diamond. In addition, during the process from S02-2 to S03-3, the front legs sequentially pose in three different configurations relative to the step: (i) rolling up the wall of the step, (ii) rotating with respect to the edge of the step and then (iii) rolling on the top. Illustrative drawings of these three scenarios are depicted in (D) lower right. Several body configurations during motion task S03 with a step height of 250 mm are plotted in this subfigure: from initial condition S02-2 (orange color), to S03-1 (light green color), where the front legs enter scenario (ii), to S03-2 (green color), where the front legs enter scenario (iii), and to S03-3 ‘measurement posture’ (dark green color). (D) Front and hind leg trajectory coordination derived from the described kinematics while the robot climbs the step with three different heights in motion task S03: 170, 210 and 250 mm. The subscripts associated with the step heights indicate the point at which the scenario changes. For example, the diamond marker with 210_{(ii)_(iii)} indicates the configurations of the front and hind legs at which the front legs change the configuration from scenario (ii) to scenario (iii). Because the three trajectories are similar and close to each other, the coordination of the front and hind legs can be approximated by a fixed trajectory, as shown by the black dashed line. In addition, the line segments encircled by a red dashed ellipse indicate the adequate leg orientations for step height measurement, as the robot reaches scenario (iii) in all three cases, with step heights 170, 210 and 250 mm.

the step, which has already been contacted. Similarly, rolling only the hind legs also yields the same result. In contrast, only rolling the front legs to lift up the body is feasible, and it is set as the ‘first action’. This action can provide the following effects: (i) generating clearance between the front of the body and the wall and (ii) adjusting the body posture until the configuration is suitable for rolling both the front and hind legs to further move the body up (i.e. four-leg-rolling motion, referred to as the ‘second action’). The switch

time from the first action to the second action is determined by the position of the body’s instantaneous COR with the four-leg-rolling condition in the sagittal plane. Basically, to feasibly perform the second action, the COR needs to be located on the upper right side of contact point P_c , as shown in figure 5(B). Thus, during the first action, the COR with the four-leg-rolling condition is computed according to the following computation order. (i) Compute the trajectory of the front hips. (ii) Compute the trajectory of the hind hips based

on the rigid body constraint with existing ground contact point P_c

$$2l_h = \sqrt{(X_{fh} - X_{hh})^2 + (Z_{fh} - Z_{hh})^2}. \quad (20)$$

(iii) Find the motion directions of the front and hind hips according to (18) and (19). (iv) Derive the instantaneous COR (X_{COR}, Z_{COR}) by finding the intersections of the normal vectors of (18) and (19). More specifically, solve the following equations:²

$$\begin{aligned} (Z_{COR} - Z_{hh}) &= -\frac{dX_{hh}}{dZ_{hh}}(X_{COR} - X_{hh}) \\ (Z_{COR} - Z_{fh}) &= -\frac{dX_{fh}}{dZ_{fh}}(X_{COR} - X_{fh}). \end{aligned} \quad (21)$$

Figure 5(B) shows the ‘virtual’ trajectory of the COR with four-leg motion (dark purple curve) during the first action, when the front legs roll up the wall (purple curve). Initially, in the S02 configuration, the point is located below the body (orange square mark). When the robot operates in the first action, the virtual COR shown in figure 5(B) moves toward the upper left direction. At a given moment, the COR, marked as the bright green square, is located above the ground contact point P_c , and this configuration represents the earliest point at which the four-leg motion (i.e. the second action) can be performed. The associated body configuration is depicted in the dashed bright green box. After this configuration, the robot switches to the second action, with a four-leg rolling motion, to push the body up. In addition, during the first action, where the front legs roll up the wall of the step, the hind legs rotate simultaneously, to keep contact with the ground, as the body inclination changes accordingly. In empirical implementation, the hind legs are programmed to push the ground a little bit to maintain ground contact.

Please note that solving the COR according to (16)–(21) assumes the second action happens while the front legs are still rolling up the wall. In general, the front legs sequentially confront three different rolling scenarios: (i) rolling up the wall, (ii) rotating with respect to the edge of the step, and then (iii) rolling on the top of the step. Thus, further development of the front hip trajectory computation should be addressed. For clear representation, the configurations when switching between scenario (i) and scenario (ii) and between scenario (ii) and scenario (iii) are hereafter referred to as S03-1 and S03-2, respectively. The trajectory of the front hip rolling according to scenario (i) is shown in (16), and that according to scenario (ii) can be represented as

$$\begin{aligned} (X_{fh}, Z_{fh}) &= \begin{bmatrix} -r_\omega \cos(\Delta\phi_f + \Delta\alpha) + (r_\omega - r_s) \sin(\phi_{fS03-1} + \alpha_{S03-1} + \Delta\phi_f + \Delta\alpha) \\ h + r_\omega \sin(\Delta\phi_f + \Delta\alpha) + (r_\omega - r_s) \cos(\phi_{fS03-1} + \alpha_{S03-1} + \Delta\phi_f + \Delta\alpha) \end{bmatrix}. \end{aligned} \quad (22)$$

² In the computation process, the rotation of front leg $\Delta\phi_f$ is the active variable, and other variables such as $\Delta\phi_h$ and $\Delta\alpha$ a, as shown in (18) and (19), can be represented as a function of $\Delta\phi_f$. Thus, $\Delta\phi_f$ is the only unknown to be solved in (21).

Similarly, the trajectory of the front hip rolling according to scenario (iii) can be derived as

$$\begin{aligned} (X_{fh}, Z_{fh}) &= \begin{bmatrix} r_\omega(\Delta\phi_f + \Delta\alpha) + (r_\omega - r_s) \sin(\phi_{fS03-2} + \alpha_{S03-2} + \Delta\phi_f + \Delta\alpha) \\ h + r_\omega + (r_\omega - r_s) \cos(\phi_{fS03-2} + \alpha_{S03-2} + \Delta\phi_f + \Delta\alpha) \end{bmatrix}. \end{aligned} \quad (23)$$

Thus, similar to the instantaneous motion direction of the front hip in scenario (i) shown in (18), that of scenario (ii) and scenario (iii) can be derived. Together with (19)–(21), the COR in these two scenarios can be correctly computed. In addition, the correct body pitch in all three scenarios can also be obtained:

$$\alpha = -\tan^{-1} \left(\frac{Z_{fh} - Z_{hh}}{X_{fh} - X_{hh}} \right). \quad (24)$$

Figure 5(C) plots several body configurations as the robot moves in motion task S03 with a step height of 250 mm, starting from S02-2 final configuration (orange color), to S03-1 (light green color), where the front legs enter scenario (ii), to S03-2 (green color), where the front legs enter scenario (iii), and to the ‘measurement posture’, hereafter referred to as S03-3 (dark green color). The purple and magenta curves represent the front and hind leg trajectories, respectively. The diamond markers represent the positions of the hips at these states.

Empirically, when the step height is above 210 mm, the front legs touch the wall of the step in the final S02-2 state. After the first action in S03 is initiated, in the case of a 220 mm step height, the front legs quickly touch the step edge and enter scenario (ii), and after a while, the second action is initiated. In contrast, in the case of a 250 mm step height, the motion in scenario (i) takes a certain amount of time, and the robot initiates the second action right after entering scenario (ii) (i.e. light green and bright green diamonds are almost at the same position as shown in figure 5(C)). If the step height is less than or equal to 210 mm (i.e. h satisfies (10)), the front legs directly catch the edge of the step (i.e. directly enter scenario (ii)), and the state can be derived as

$$\begin{aligned} \phi &= \sin^{-1} \left(\frac{Z_{fhS02-2} - (r_\omega - r_s) \cos(\phi_{fS02-2} + \alpha_{S02-2}) - h}{r_\omega} \right) \\ (X_{fh}, Z_{fh}) &= \begin{bmatrix} -r_\omega \cos(\Delta\phi_f + \Delta\alpha + \phi) + (r_\omega - r_s) \sin(\phi_{fS02-2} + \alpha_{S02-2} + \Delta\phi_f + \Delta\alpha) \\ h + r_\omega \sin(\Delta\phi_f + \Delta\alpha + \phi) + (r_\omega - r_s) \cos(\phi_{fS02-2} + \alpha_{S02-2} + \Delta\phi_f + \Delta\alpha) \end{bmatrix}. \end{aligned} \quad (25)$$

With (16)–(25), the kinematics of the robot motion in S03 can be successfully simulated, no matter how tall the step is or what type of motion the robot goes through, starting from S02. Empirically, however, because the robot does not know the height of the step before it reaches the measurement posture in S03-3, planning different maneuvers to climb steps of different

heights is unrealistic (i.e. the robot does not know which trajectories to use—scenario (i), (ii) or (iii)). Thus, evaluating whether it is possible to find a pre-planned trajectory suitable for the robot to climb steps of different heights is the crucial task.

Figure 5(D) plots the trajectory coordination between the front and hind legs based on the described kinematic analysis while the robot climbs steps of three different heights (170, 210 and 250 mm) from the S02-2 state (figure 5(C) in orange color) to the S03-3 state (figure 5(C) in dark green color). This figure reveals an important fact: although the front legs may move through three significantly different scenarios (i)–(iii) due to different step heights, the trajectory coordination between the front and hind legs are roughly the same. Together with the fact that the leg trajectories in S02 are irrelevant to the step height, we can conclude that it is feasible to utilize one pre-designed trajectory for the robot from the initiation of the step-climbing maneuver until it arrives at the ‘measurement posture’. This characteristic is crucial because the step height is unknown before the step height measurement. Without knowing the step height, planning different maneuvers to climb steps of different heights is unrealistic. Thus, a pre-defined and approximated trajectory, shown as a black dashed line, is utilized for all scenarios in the empirical implementation. Figure 5(D) also depicts the timing of switching among different scenarios in diamond markers. For 170 mm high or 210 mm high steps (and any other heights in between), the motion of the front legs directly enters scenario (ii) (i.e. rotating with respect to the edge of the step); thus, only one diamond marker appears on the curve, indicating the transition from scenario (ii) to scenario (iii). In contrast, the robot goes through three scenarios when climbing high steps. For example, two diamond markers exist on the 250 mm curve. The plot reveals that the line segment encircled by a red dashed ellipse can be the adequate leg orientations for step height measurement, where the robot reaches scenario (iii) in all cases. In the empirical implementation, the robot stops for a short amount of time at the S03-3 configuration for height measurement. Due to slippage in the ground contact and slight body vibration due to leg compliance, the step height is measured twice to improve accuracy—one soon after the other, with little body movement. The detected step height, h , is utilized to determine the accurate trajectories of the legs in the next motion, S04.

S04: Rising stage part II—fine body posture adjustment. After the front legs arrive at the top of the step, the body lift relies primarily on the motion of the middle and hind legs. For climbing a low step, these four legs have equivalent importance. The middle legs catch the edge of the step, and the hind legs push against the ground to lift the body up in coordination. In contrast, when climbing high steps, the middle legs are more vital than the hind legs, as there are certain moments when the hind legs lose ground contact before the body is fully lifted. Thus, how to correctly adjust the body posture so the middle legs can engage the edge of the step plays a vital role. No matter how high the step is, the body configuration, especially the middle hips, should be set as close to the edge of the step as possible for two purposes: (i) to enable the middle legs to engage the step effectively, and

(ii) to move the COM close to the step. To achieve this goal, the first motion is to move the body close to the edge of the step by rotating the front and hind legs. The amount of rotation depends on measured step height h . Next, for step heights lower than or equal to 210 mm, the middle leg engages the step, and the hind legs rotate a little in a clockwise direction to adjust the body inclination, preparing for the body lift (hereafter referred to as the ‘210 mm algorithm’). For steps higher than 210 mm, an extra rotation of the hind legs is performed to further move the body close to the step, so the middle legs can be close enough to engage the edge of the step (hereafter referred to as the ‘250 mm algorithm’).

The quantitative analysis of S04 with the 210 mm algorithm is detailed as follows. With the assumption of pure four-leg-rolling motion and the known initial conditions $(X_{fh}, Z_{fh})_{S03-3}$ and $(X_{hh}, Z_{hh})_{S03-3}$, the body inclination, m , can be quantitatively computed as a function of $\Delta\phi_h$,

$$m = f_{S04-1}(\Delta\phi_h) = \frac{Z_{fh} - Z_{hh}}{X_{fh} - X_{hh}}. \quad (26)$$

The distance from the hip line to the edge of the step, d_e , shown in figure 6(A), can then be computed as

$$d_e(\Delta\phi_h) = \frac{|Z_{hh} - mX_{hh} - h|}{\sqrt{m^2 + 1}}. \quad (27)$$

With the setting $d_e = h_h$ (i.e. the bottom of the body touches the edge of the step), the required hind leg rotation $\Delta\phi_h$ can be derived, and the body configuration can then be quantitatively derived by (26) (hereafter referred to as S04-1). Next, the middle legs rotate to configuration ϕ_m to engage the edge of the step, and ϕ_m can be calculated in a similar manner as the front legs, shown in (11). The hind legs then rotate a little in a clockwise direction so the body can pose with adequate inclination in preparation for lifting (referred to as S04-2a). The horizontal distance of the tips of the hind legs at this configuration can be computed as

$$X_{ht} = X_{hh} + (r_\omega - r_s) \sin(-(\phi_h + \alpha)) + r_\omega \cos(\frac{3}{2}\pi + \phi_h + \alpha - \phi_l), \quad (28)$$

where ϕ_l is the dimension of the robot legs shown in figure 1(B). Equation (28) indicates how close the leg is to the step wall, and this information is used in the following motion task, S05. Figure 6(A) plots the overall S04 motion with a step height equal to or lower than 210 mm. In an empirical setting, a body inclination of 70 degrees is preferred right before the body lift in motion task S05.

The quantitative analysis of S04 with the 250 mm algorithm is detailed as follows. The first motion to bring the body close to the edge is the same as the 210 mm algorithm shown in (26) and (27). Because of the high step height, even when the body has touched the edge of the step, as in the S04-1 configuration, the middle legs are still too far from the edge to perform a feasible engagement. Thus, the hind legs are programmed to rotate and bring the body closer to the step. Based on the assumption of pure rolling of the hind legs, the hind hip coordinate (X_{hh}, Z_{hh}) can be derived with the given

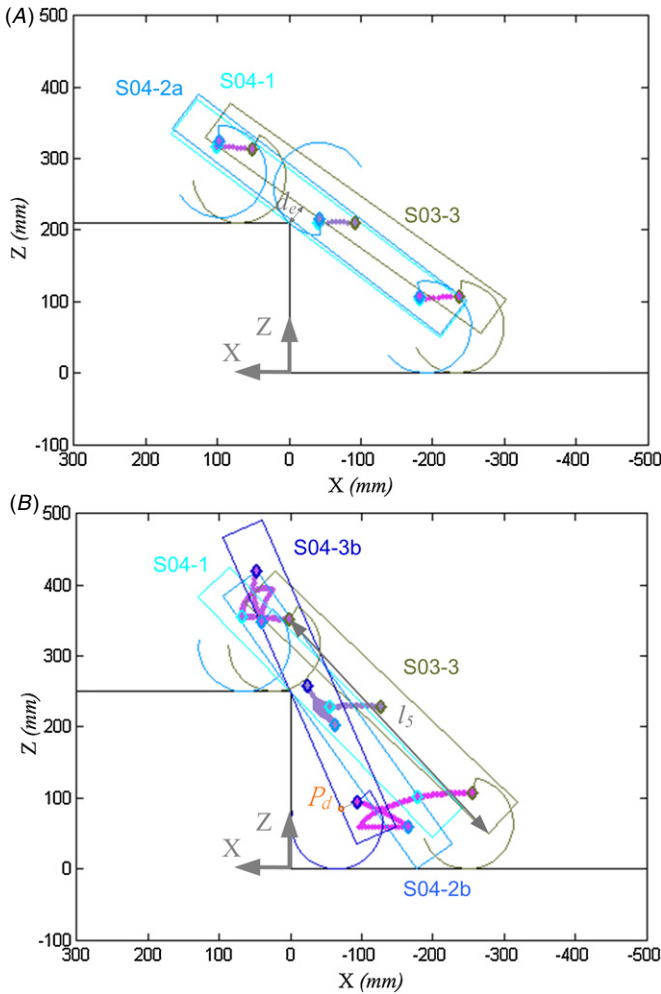


Figure 6. S04, rising stage part II—fine body posture adjustment: (A) several body configurations during motion task S04 with 210 mm step height. (B) Several body configurations during motion task S04 with 250 mm step height.

initial condition $(X_{hh}, Z_{hh})_{S04-1}$. During the motion, the body pitch angle can be computed as the function of the step height,

$$\alpha = -\tan^{-1}\left(\frac{h - Z_{hd}}{-X_{hd}}\right), \quad (29)$$

where $P_d = (X_{hd}, Z_{hd})$ is the point located at the bottom of the body and vertically below the hind hip in the body coordinate, as shown in figure 6(B). Its position can be derived according to the geometrical relations

$$\begin{aligned} (X_{hd} - X_{hh})^2 + (Z_{hd} - Z_{hh})^2 &= h_h^2 \\ \frac{Z_{hd} - Z_{hh}}{X_{hd} - X_{hh}} \times \frac{Z_{hd} - h}{X_{hd}} &= -1. \end{aligned} \quad (30)$$

The hind body touches the ground when

$$Z_{hh} = \sqrt{l_t^2 + h_h^2} \sin\left(-\alpha + \tan^{-1}\left(\frac{h_h}{l_t}\right)\right). \quad (31)$$

At this moment, the robot is supported by a small contact point. Because of low contact friction, the body slides down a

little bit until the front legs catches the step top at

$$\begin{aligned} Z_{fh} &= h + r_\omega + (r_\omega - r_s) \cos(\phi_f + \alpha_{S04-2b}) \\ \alpha_{S04-2b} &= -\sin^{-1}\left(\frac{Z_{fh}}{l_5}\right) + \tan^{-1}\left(\frac{h_h}{2l_h + l_t}\right), \end{aligned} \quad (32)$$

with

$$l_5 = \sqrt{(2l_h + l_t)^2 + h_h^2}.$$

The body state in this configuration is hereafter referred to as S04-2b. The configuration of the hind legs to re-contact the ground can be computed according to (28), and the quantitative computation of the re-standing motion is similar to that shown in (29) and (30), and is referred to as S04-3b. Figure 6(B) plots the overall S04 motion with a step higher than 210 mm, according to the algorithm shown above.

S05: Rising stage part III—the body lift-up. After the fine body posture adjustment executed in motion task S04 to engage the middle legs, now the robot is ready for lift-up. For the 210 mm algorithm, the action is merely the continuous rotation of the middle legs to pull the body closer to the step and then lift the body upward and forward. For the 250 mm algorithm, the middle leg motion directly lifts the body upward and forward, as the hind legs are already in contact with the wall of the step in S04-3b. For both cases, during the body lift, when the horizontal projection of the robot COM on the step passes the ground contact points of the middle legs, the robot body falls onto the step due to gravity (hereafter referred to as the ‘free-fall’). During the free-fall, the compliant front legs are configured to contact the ground first in order to absorb the impact force, preventing the direct impact of the robot body with the ground.

The quantitative analysis of S05 with 210 mm algorithm is detailed as follows. When the middle legs of the robot rotate, the body is pulled toward the wall of the step. The trajectory of the middle hip (X_{mh}, Z_{mh}) can be quantitatively calculated based on the assumption of rolling contact (light purple curve shown in figure 7(A)). Together with the setup of fixed hind leg orientation and the continuing contact between the hind legs and the ground, the trajectory of the hind leg center (X_{hc}, r) can be computed based on the rigid body constraint

$$(X_{mh} - X_{hc})^2 + (Z_{mh} - r)^2 = l_{hc2mh}^2, \quad (33)$$

where l_{hc2mh} is the distance between the hind leg center and the middle hip. Then, the horizontal coordinate of the hind leg tip can be computed:

$$X_{ht} = X_{hc} + r_\omega \cos\left(\frac{3}{2}\pi + \phi_h + \alpha - \phi_l\right). \quad (34)$$

At a certain point, the hind hip touches the wall of the step ($X_{ht} = 0$), and the body configuration can be quantitatively solved by (33)–(34), hereafter referred to as S05-1a. While the middle leg continues rotating, the robot body is lifted up so that the underside of the body contacts the edge of the step and the hind legs touch the wall. During the body lifting motion, the wall, the robot body and the hind legs form a specific geometry

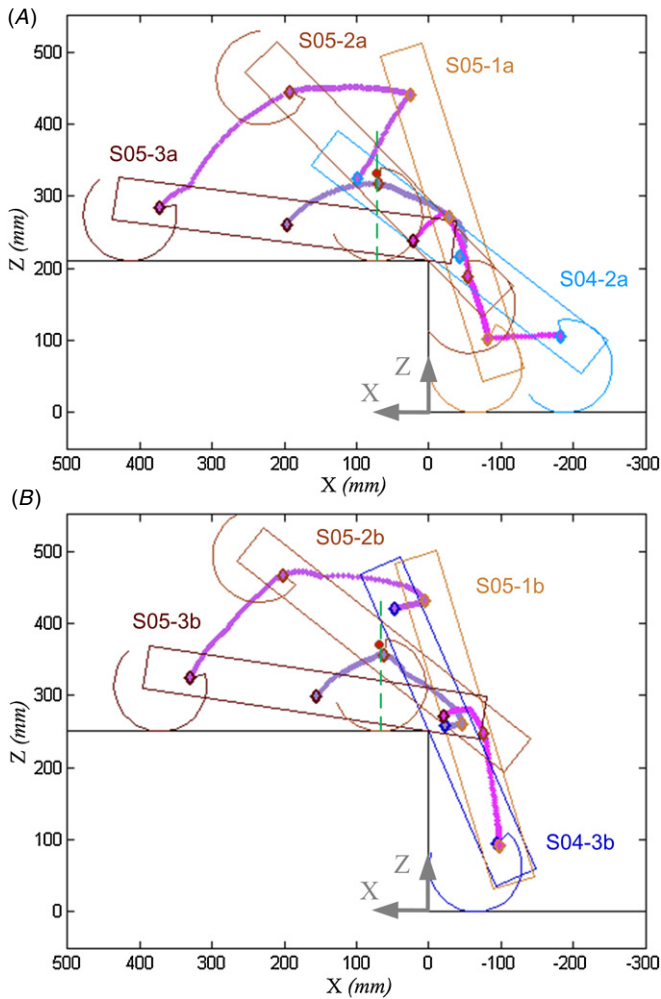


Figure 7. S05, rising stage part III—the body lift-up: (A) several body configurations during motion task S05 with 210 mm step height. (B) Several body configurations during motion task S05 with 250 mm step height. The purple, light purple and magenta curves represent the front, middle and hind hip trajectories, respectively.

and determine the body pitch angle. The computation process is similar to (29) and (30) and is skipped. During the lift-up, the rotation of the middle legs gradually moves the body COM forward and decreases the body pitch angle, but slippage behavior is observed, due to the geometry constraint described above. After the COM passes the ground contact point (dashed green lines shown in figures 7(A) and (B)—the configuration is referred to as the S05-2a),

$$X_{\text{COM}} > X_{mh} - (r_w - r_s) \sin(\phi_m + \alpha), \quad (35)$$

the body falls on the step with respect to the rolling of the middle legs as the pivot point (referred to as S05-3a). Figure 7(A) plots the overall S05 motion of the 210 mm algorithm, which clearly shows the maneuver of the robot body and the trajectories of the hips. For the 250 mm algorithm, because of the high step height, the rotation of the middle legs initially pushes the body and the hind legs a little bit away from the edge of the step and then pulls the body toward the step (referred to as S05-1b). At this moment, the hind legs touch the step and the configuration is similar to that of

S05-1a, described above. Therefore, the following body lift motion is also similar to that of the 210 mm algorithm, and the quantitative computation can be executed in the similar manner. Figure 7(B) plots the overall S05 motion of the 250 mm algorithm, starting from S04-3b as the initial condition to S05-1b, where the hind legs retouch the step, to S05-2b, where the COM pass the ground contact point, and to S05-3b, where the body falls onto the top of the step.

The robot body posture adjustment described in motion task S04 before the body lift in S05 is necessary. For climbing steps lower than or equal to 210 mm, if the orientations of the hind legs do not adjust as in the described action from S04-1 to S04-2a, the robot poses with a higher inclination, as the initial posture for motion S05. As a result, during the body lift motion in S05, the robot COM is pulled mainly upward, but not forward, to the top of the step, and the COM is not maneuvered to pass to the edge of the step. After the half-turn rotation of the middle legs, at which point they lose contact with the step, the robot falls. When climbing steps higher than 210 mm, if the hind legs do not perform the extra rotation to move the body closer to the wall of the step in the described action from S04-1 to S04-3b, the rotation of the middle legs in motion task S05 is not capable of lifting the body up completely, since the effective rolling distance of the half-circle legs in this configuration is limited. After the half-turn rotation of the middle legs, at which point they lose contact with the step, the robot falls. In summary, the robot body posture adjustment described in motion task S04 before the body lift cannot be skipped.

S06: Body configuration check and adjustment. Because in the proposed algorithm the legs only contact the wall and the top surface of the step near the edge, the algorithm is also applicable to bar-shape obstacles. In terms of mathematical formulation, the bar and the step can both be treated as rectangular functions, one with finite width, and the other with infinite width. Thus, the algorithm to maneuver the robot COM from the lower level to the upper level of either a bar or a step is, in principle, identical. However, the configuration of the robot after free-fall in motion S05 may appear different, which depends on the shape of the obstacle, bar or step. Because the front legs are posed to absorb the impact of free-fall, the final configuration of the robot on the step is inclined with head side up. If the robot climbs a bar of moderate width, it may 'sit' on the top bar after free-fall and pose horizontally. If the robot climbs a narrow bar, the final configuration is inclined with head side down. All three scenarios are depicted in figure 2. Due to the clear posture difference after free-fall, the inclinometer installed on the robot body can be utilized to categorize the shape of the obstacle (i.e. step, bar or narrow bar) and to determine the following leg motion to correct the posture. For a step, the robot releases the front legs to lay the body horizontally, preparing for standing up in the next motion task S07. For a bar and narrow bar, the legs are rotated to push the body, moving forward and climbing the bar completely. Because of gravity, the maneuver of the robot down the bar is straightforward and robust. After the maneuver in S06, the robot lies horizontally on the surface.

S07: Stand-up and tripod walking. The robot stands up and moves forward with the normal tripod gait.

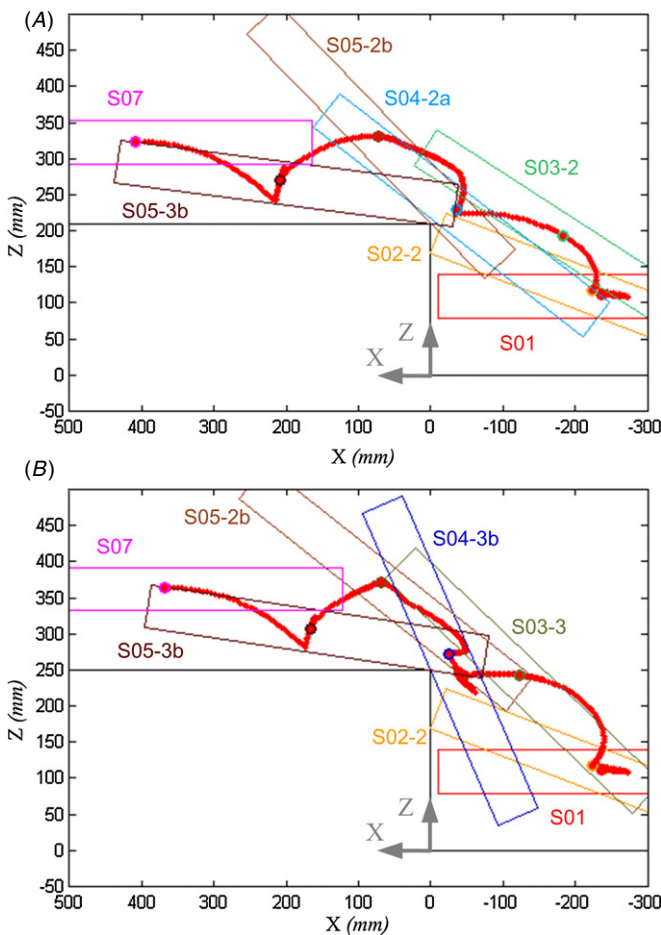


Figure 8. Robot COM trajectories (red curves) with several body postures as the robot crosses a step with a height of (A) 210 mm or (B) 250 mm from the initiation of the step-climbing maneuver described in motion task S01 to the re-standing-up behavior described in motion task S07.

Motion tasks S01 to S07 represent the proposed bio-inspired motion sequences the robot performs to climb a step higher than the upper limit at which the robot can climb with a normal tripod walking gait. Motion tasks S01 to S07 provide the right sequence of leg motions, which generate adequate force interaction with the step so that the robot COM can be successfully maneuvered to arrive at the top of the step or to climb the bar. Figures 8(A) and (B) depict the overall kinematic simulation of the COM trajectories and body orientations of motion tasks S01 to S07, wherein the robot performs the step-climbing behavior with 210 mm and 250 mm high steps, respectively.

3. Discussion: animal versus robot

Legged morphology was widely adopted in ground animals after a long evolutionary process, and the design of legged robots is in general inspired by these biological systems. However, the bio-inspired process, by definition, is not biomimetic work that tries to copy the biological systems completely; rather, it extracts the essential adoptable concepts for engineering systems. One of the significant differences between multi-legged animals and robots is the number of

active DOFs. Legged animals in general have limbs with very high DOFs, yet with sufficient power density. With a sophisticated neurocontroller, animals are capable of rapid, agile and stable locomotion on rough terrains. In contrast, legged robots usually have fewer DOFs, because today's technology limitations constrain controller complexity and power density of actuators. Thus, bio-inspired locomotion in robots has to undergo adequate modification of the original principles so that the locomotion can be successfully performed by the robotic systems. For example, the idea of template and anchor clearly defines the relationship between the original morphology and feasible control principle (Full and Koditschek 1999).

For step-climbing, the adequate maneuver of COM to climb a high step, intuitively, is lifting the COM gradually while maintaining forward motion if the high step is detected a couple of steps ahead. Perhaps owing to limited sensing capability, the cockroach tends to maintain its tripod walking gait for forward motion, and it does not change its gait unless it bumps into a step when it is too high to pass. At this instant, the forward motion ceases, and the regenerated motion focuses on rearing the body, lifting the COM, and then moving forward. The rearing stage utilized by the cockroach (Watson *et al* 2002b) can (and should) be adopted for robotic systems (i.e. motion task S02), as the underlying principle is strongly supported by the physical sense: the front side of the body needs to be tilted up so the front legs can catch the top of the step more easily. The rising stage utilized by the cockroach to lift the COM with little or no further change of body inclination is a challenge in the RHex-style robot because of the low DOFs of the legs. Thus, the rising and forward motion after the rearing motion is interpreted at the bio-inspiration level as finding the adequate maneuver of the COM in the robotic system, based on leg actuation force and gravity. Therefore, motion tasks S03–S05 described in section 2 were developed. Because of the limited active DOFs, not only is the motion planning a challenge, but also the maneuver of the COM may be constrained to behave in a certain manner. For example, for the former, the posture adjustment in S04 is necessary. For the latter, in the process of shifting the COM further forward (i.e. motion task S05) to let the robot body lie stably on the top of the step, the COM is inevitably lifted to a height much higher than the top of the step, as shown in figure 7. This motion is not power-efficient, due to the required extra energy for raising the body's potential energy. However, body lift-up by the middle legs seems to be the only feasible method to successfully maneuver the robot COM to pass the edge of the step further, and a simple rotation motion generates simultaneous forward and upward locomotion. This is the trade-off of a robotic system with low DOFs: it is a robust system, but with constrained maneuverability. In addition, the seemingly easy lifting displayed by the cockroach becomes a nontrivial maneuver in the robot in the rising stages, detailed in motion tasks S03 to S05, which require certain quantitative analysis to develop the feasible leg motion sequence.

Watson *et al* reported that cockroaches (*B. discoidalis*) have at least four other climbing strategies in ascending higher obstacles (~30% in total) besides the commonly used

rearing/rising strategy described above ($\sim 70\%$) (Watson *et al* 2002b). These strategies are: (1) *elevate*, ‘simultaneously extending all six legs to produce an elevation of the whole body’. This method is not feasible in the RHex-style robot because it has only one rotational DOF per leg, and the body cannot be lifted up by the legs with limited leg trajectory space; (2) *jump*, this method is not adopted due to limited actuator power density of the robot. (3) *head-butt* (i.e. brute force, $\sim 10\%$), ‘simply butt the head against the block thereby forcing the body upward’. This process involves soft body deformation and is only suitable for climbing low obstacles. (4) T1 leg on top ($\sim 11\%$), ‘using an unusually high swing trajectory for one front leg in order to place it on top of the block while keeping the body horizontal’. This behavior is also suitable for climbing low obstacles.

The locomotion of RHex-style robots using an open-loop tripod walking gait to pass obstacles is basically a combination of normal tripod walking, (3), and (4), described in the previous paragraph. Due to the open-loop locomotion and the design of the full-rotation recovery of the legs in the tripod walking gait (i.e. Buehler clock (Saranli *et al* 2001)), when the robot confronts an obstacle, it either bumps into the obstacle (i.e. strategy (3)) or directly climbs up the obstacle using leg rotation (strategy (4)), depending on the relative configurations of the obstacle, the robot and the legs. The tripod walking locomotion in the RHex-style robot is quite effective when the obstacles are not high. However, this method is not feasible when the obstacle is too high for the front legs to reach. In this situation, the robot should use the rearing/rising strategy, as the developed work shown in this paper, as cockroaches do in most situations ($\sim 70\%$). In summary, with the combination of normal tripod walking and the work presented in this paper, the bio-inspired behaviors of the robot covers $\sim 90\%$ of the behaviors of the cockroach when it encounters steps.

4. Experimental evaluation

The RHex-style robot shown in figure 1(A) was built for experimental evaluation of the proposed step-climbing algorithm. The dimensions are presented in figure 1(B). A real-time embedded control system (sBRIO-9602, National Instruments) running at 1 kHz together with integrated FPGA running at 10 kHz serves as the main computation power on the robot. The onboard inertial measurement unit (IMU) is comprised of one 3-axis accelerometer (ADXL330, ± 3 g, Analog Device) and three 1-axis rate gyros (ADXRS610, ± 3000 s⁻¹, Analog Device). A 2-axis inclinometer (SCA100T, ± 900 , VTI Technologies) was installed for body inclination detection. Two IR range sensors (GP2D120XJ00F, Sharp) were installed on the front of the robot to detect obstacles. The analog sensory signals were collected by AI module (NI-9205, National Instruments), which has 32 analog input channels with 16-bit A-to-D resolutions.

The experimental data was collected while the robot climbed a step within the ground truth measurement system (GTMS), shown in figure 9. The system has two high-speed cameras (A504 k, Basler) installed on the top right and left

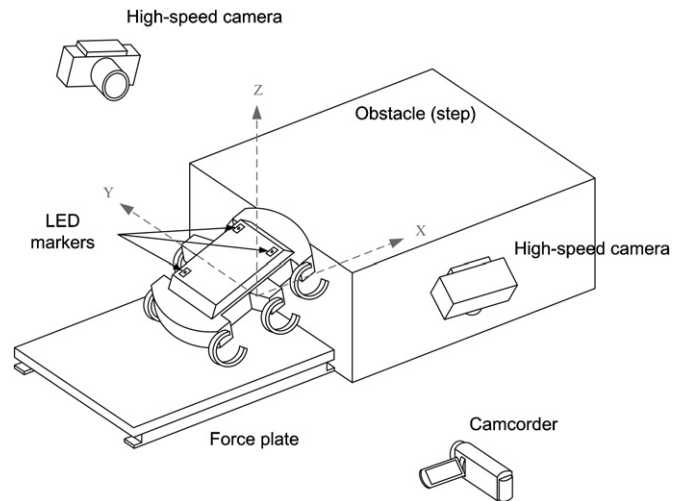


Figure 9. Experimental evaluation setup for the robot performing the step-crossing behavior.

Table 3. Statistical results of the robot climbing steps.

Obstacle-height (mm)	Success rate (%)	Mean and std of measured heights (mm)/(mm)
210 mm algorithm		
150	100	150.1 (2.6)
160	100	159.4 (3.1)
170	100	168.4 (1.1)
180	100	178.9 (1.7)
190	100	190.7 (1.4)
200	100	199.6 (1.6)
210	100	209.6 (1.7)
215	100	215.3 (1.2)
220	70	219.8 (1.4)
250 mm algorithm		
220	100	219.5 (2.1)
230	100	230.5 (2.7)
240	100	239.2 (2.2)
250	100	250.0 (3.0)
260 ^a	0	258.8 (2.4)
270 ^a	0	268.1 (2.0)

^aThe test is for evaluation purpose. In the empirical implementation, when the step height measured by the robot is above 250 mm, the robot is programmed to perform the safe-return mode, which entailed climbing down the step and walking away.

sides of the experimental area to capture three LED markers mounted on top of the robot. The 3D positions of the markers can be reconstructed by two synchronized images captured by the cameras, running at 200 Hz. The COM trajectories and the body orientations versus time were recovered by the computed 3D coordinates of the three markers. The force plate (4060-07-1000, Bertec) was placed on either the bottom or the top of the step to record the force interaction between the robot and the step. A camcorder (HDR-XR350, SONY) recorded the robot climbing motion from a side view. Right after the robot climbed the step, the LED markers were turned off, and the on/off timing was utilized for synchronizing the robot's data (IMU, inclinometer and encoder), the force plate, the high-speed cameras and the camcorder.

Table 3 lists the statistical results of the robot climbing steps of various heights. Success rate is the average of ten test

runs. The measured height is the average of the *in situ* height measurements by the inclinometer. The data reveal that with the 210 mm algorithm, the robot was able to climb steps with heights up to 210 mm with a 100% success rate, and 220 mm steps with a 70% success rate. The failure in the high step is because the robot COM was not maneuvered to the right side enough to enable a safe landing for the robot. Thus, the robot fell to the bottom of the step when the middle legs finished their rotational motion and disengaged the top of the step in motion S05. The 250 mm algorithm was utilized for steps higher than 210 mm, and the robot was able to climb steps up to 250 mm high with 100% success rate, but it had no success at 260 mm and 270 mm. The extra rotation of the hind leg utilized in motion S04 pulled the body close to the step, so the robot body could be posed in a better configuration to be maneuvered and lifted correctly by the rotation of the middle legs. When attempting to climb steps higher than 250 mm, although the revised 250 mm algorithm moved the body close to the step, the middle legs of the robot were not able to engage the edge of the step in the right manner to lift the body up, due to the size of the robot relative to the step (i.e. geometrical limitation). The major failure mode in this case is pitch-over. The onboard inclinometer could detect the event of falling by checking direction of gravity. However, due to limited leg maneuverability, there was no easy way to recover this failure and continue climbing. Therefore, when the step height measured by the robot was above 250 mm, the robot was programmed to perform the safe-return mode, which entailed climbing down the step and walking away, as described in the flow chart of the robot motion sequence shown in figure 2. A dynamic maneuver, such as jumping, would be required for the robot to climb a step that high. The 250 mm algorithm can be utilized to climb steps 150–210 mm in height. However, in this case, the time required for step climbing is longer, and the body contacts the step or the ground a couple of times, which is not preferable. Thus, the overall algorithm is divided into two sub-routines, according to step height, as shown in figure 2 and described in S04. In summary, the robot was able to reliably climb steps up to 250 mm high, more than twice the 107 mm leg length (230%) and 70% longer than its body height in a standing posture.

Figure 10 shows the sequential images extracted from a typical video recording demonstrating the robot automatically climbing a 250 mm high step. The sequence of motion is as follows. (A) The robot walked toward the step. (B) After the IR ranges sensed the existence of the step, (C) the robot stopped walking and started the step-climbing behavior. First, (D) the middle legs moved to shift the ground contact point forward. After retracting the hind legs, (E) the body tilted. Because the IR signals also indicated that the robot was not perpendicular to the wall of the step, (F) the posture was corrected by middle leg propulsion. (G) After the front legs grabbed the wall, (H) the body was lifted for the first and (I) second step height measurement. (J) The measured 250 mm step height induced the extra rotation of the hind leg (K) to bring the body close to the step. (L) The middle legs caught the edge of the step and (M) began the body lift-up. (N) The resulting free-fall let the robot body lie stably on top of the step. (O) After posture

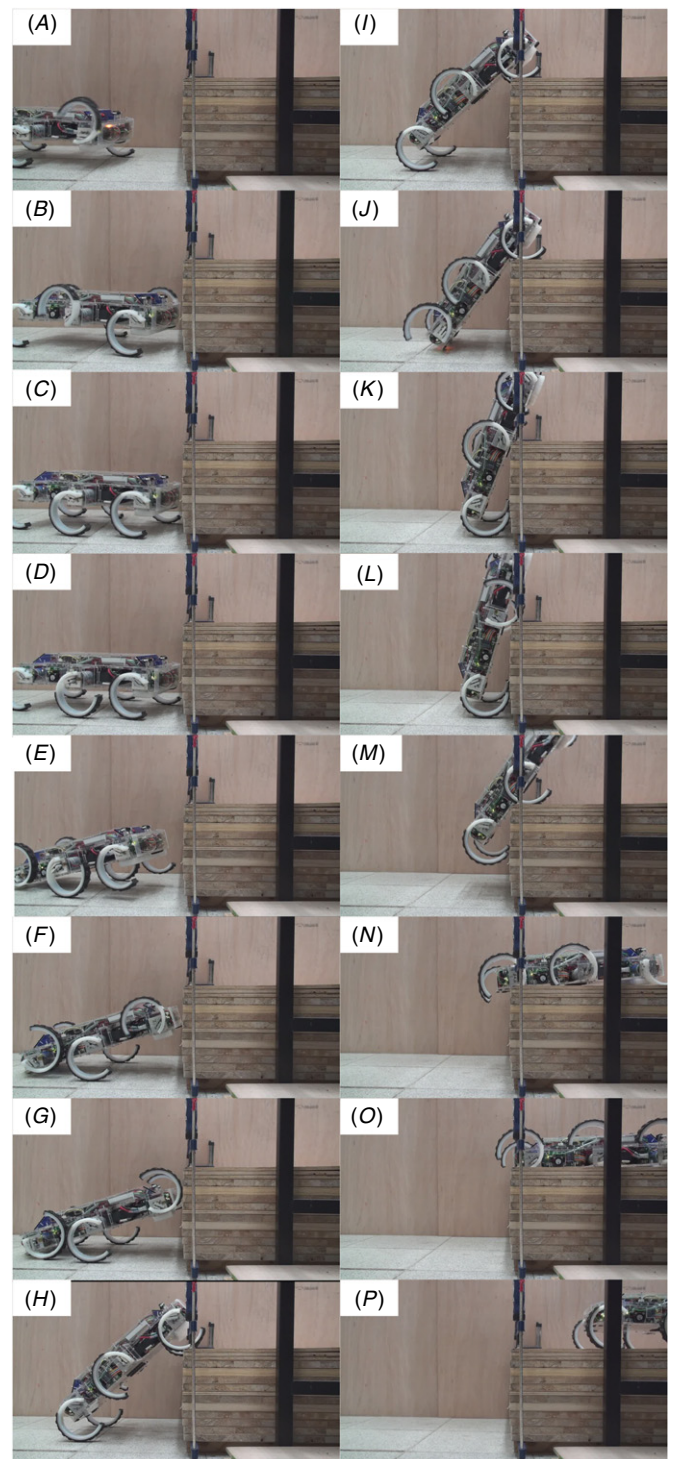


Figure 10. Sequence of images extracted from a typical video showing the robot crossing a 250 mm high step.

adjustment, (P) the robot stood up for tripod walking. This figure confirms the effectiveness of the step-climbing behavior. The full video is available as a media extension associated with this paper. Videos of the robot performing step climbing in different scenarios are also available as media extensions.

Figure 11 plots the experimental results of the COM trajectories measured by the GTMS while the robot climbed the 250 mm high step. Figure 11(A) shows the 3D COM trajectory (purple curve), which is the mean of several test runs.

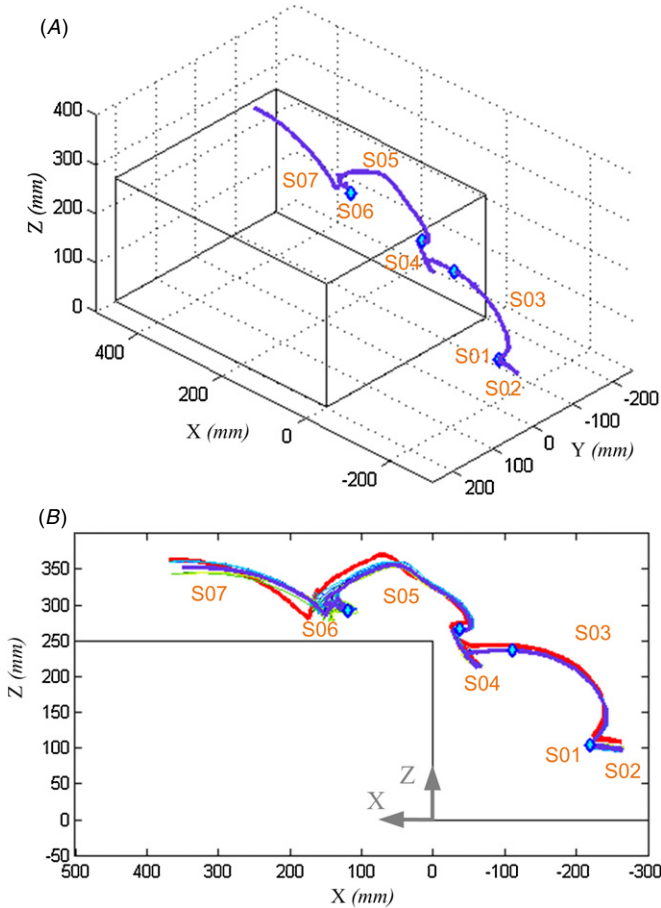


Figure 11. The robot COM trajectories measured by the GTMS while the robot crossed the 250 mm high step in (A) three-dimensional plot and in (B) a sagittal-plane plot. The notations correspond to motion tasks S01–S07 described in section 2. The purple curves represent the averaged COM trajectory, and the trajectories of individual experimental runs are plotted in various colors. The red curve depicted in (B) represents the computed COM trajectory for comparison, which is identical to the curve shown in figure 8(B).

Because the trajectory is designed in a sagittal plane, and in the empirical implementation, the right and left legs are actuated simultaneously with position control, the trajectory is close to planar, as expected. The trajectory sections corresponding to motions S01 to S07 described in section 2 are also marked. The motions all involve maneuvering the robot COM, except for S01 and S06, which are status-checking motions. The initial inclination in S02 (rearing stage) moved the COM backward a little bit, and the following forward motion with maintained inclination shifted the COM back to a position close to the original location. The major change in motion S02 is the body inclination, similar to the behavior of cockroaches in the rearing stage. The first rising stage in motion S03 shifted the COM up so the front legs could grasp the top of the step for step height measurement. The rising stage in motion S04 adjusted the body posture so the robot COM could move close to the edge of the step. The final rising stage in motion S05 lifted the body up, and then the body fell stably on top of the step. Standing-up motion S07 moved the COM upward and forward simultaneously, due to the rolling contact of the half-

Table 4. Root mean-squared error between the kinematic simulation and averaged experiment results.

Motion task	S02	S03	S04	S05	S07	All
RMS (mm)	10.9	6.5	7.3	12.3	12.1	10.1

circle legs. Figure 11(B) plots the planar trajectories of the test runs (thin curves in various colors), their mean (purple curve) and the kinematic simulation (red curve) described in section 2. The associated root mean squared (RMS) error between the kinematic simulation and the averaged experimental results are listed in table 4. The small variation among test runs validates the repeatability and robustness of the proposed algorithm in the empirical evaluation. The region with slightly larger variation right before S06 is a result of the impact and body bounce during and after the free-fall. Comparing the mean of the experimental trajectory to the kinematic simulated one, the trajectories in most of the sections match quite well. The trajectory difference in motion S05 was caused by the slippage of the middle legs when it began to lift the body up, resulting in the backward sliding of the robot body. Because of the same slippage, the pivot point changed during the free-fall, resulting in a trajectory difference in the free-fall section and the following standing posture as well. Thus, the RMS errors after S05 are all above 10 mm. In summary, the RMS error of the overall motion is 10.1 mm, 2% of the body length. The adequate match of the experimental trajectories to the simulated one confirms that the proposed trajectory design is feasible and applicable in a real situation.

Figure 12 shows the vertical and horizontal forces versus time while the robot climbed the 250 mm high step. The dark blue and green lines are the means of several experimental measurements of the force plate installed at the bottom and the top of the step, respectively. The light blue and green bars indicate the standard deviations of these force measurements at several sampled timings. The light brown line represents the resultant force interacting between the robot and the ground (i.e. green + blue). Because only one force plate was available for the experiment, these two curves are composed of results from different experimental data sets, and the curves are synchronized based on the static posture, shown in figure 5(A), when the robot took the step height measurement. At this posture, the summation of the vertical forces should be equal to the weight of the robot. For the vertical force measurement shown in figure 12(A), it is reasonable to have force only on the bottom plate during motions S01 and S02. After the front legs caught the edge of the step in motion S03, the vertical force gradually transmitted from the bottom force plate to the top one. During the static posture shown in figure 5(A), the forces on both plates were roughly equal, which can be derived from static engineering mechanics. In the posture adjustment in motion S04, however, the force transmitted back to the lower plate because the robot mainly sat on the bottom force plate. The major force transmission for body lift from the bottom plate to the top plate happened in motion S05, after which the bottom force plate had no contact force. The big force vibrations in S06 and S07 were caused by the impact of the front legs with the ground after

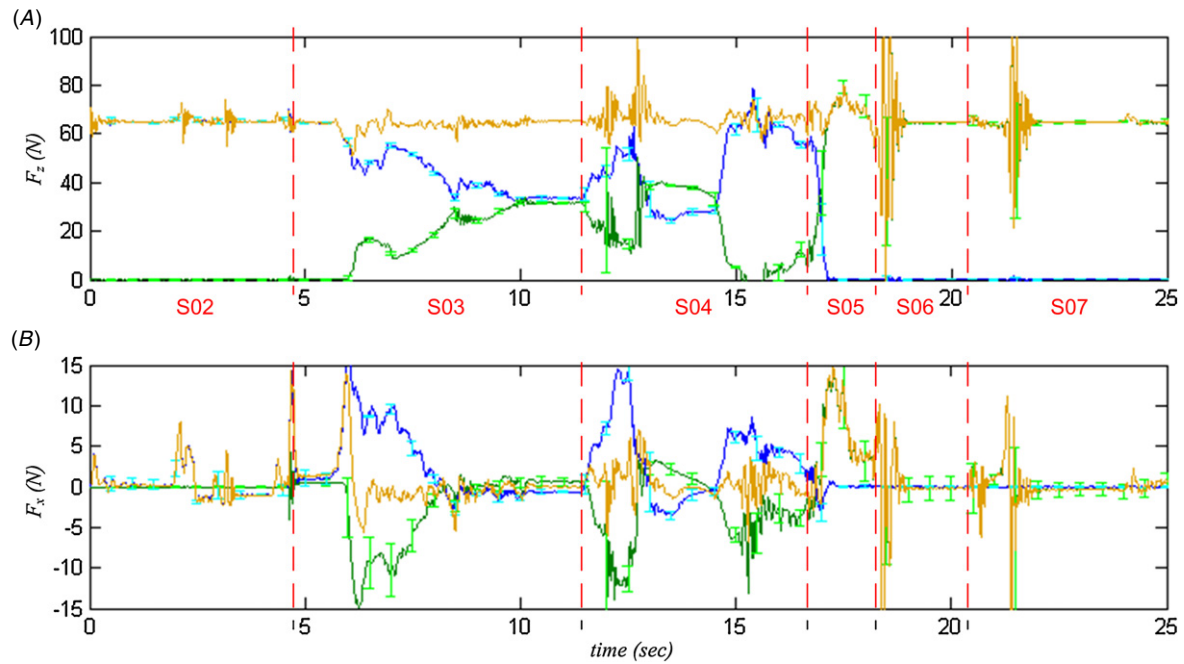


Figure 12. The vertical (A) and horizontal (B) forces versus time while the robot crossed the 250 mm high step. The dark blue and dark green curves represent the averaged measurements from the lower and upper force plates, respectively. The light blue and green bars indicate the standard deviations of these force measurements at several sampled timings. The light brown line represents the resultant force interacting between the robot and the ground (i.e. green + blue). The positive values indicate the upward and forward ground reaction forces to the robot.

free-fall, and the impact of the body to the ground after the release of the front legs. The standard deviation of the forces during the climbing is small compared to the means, which indicates the repeatability and consistency of the climbing motion. Similarly, for the horizontal force measurement shown in figure 12(B), it is reasonable to have force only on the bottom or top force plates during motions S01&S02 and S06&S07, respectively. The step-climbing motion is close to quasi-static, so the resultant forward force is small. Except for the peaks resulting from the impacts, three meaningful resultant forward forces are: (i) moving the body forward in the rearing stage S02; (ii) initial engaging of the top force plate for height measurement in S03; and (iii) the major body lift-up in S05, which has the largest forward propulsion magnitude and time duration. The forward and backward forces of large and opposite magnitudes that appeared in the bottom and top force plates indicate the push and brake interaction during climbing. These forces might result from the mixed effects of the position control and the leg compliance, and this interaction, to a certain degree, provides the ‘locking’ of the robot to the ground, thus providing a more stable and repeatable climbing behavior. A similar behavior can be observed in the climbing cockroach, which uses its middle legs to generate pull-in force toward the body (Goldman *et al* 2006).

Figures 11 and 12 also confirm that the developed step-climbing maneuver is basically quasi-static, except for the free-fall in S05 rising stage part III, the body lift-up, as the empirical robot trajectories are similar to the developed kinematic-based trajectory. Although the kinematic analysis is not as realistic as dynamics, it is straightforward and feasible, yet sufficient to yield adequate performance. On the other hand, the leg

maneuver for the robot to climb high steps is not trivial, either. Due to strong geometric constraints, generating adequate trajectories would require underlying physics principles and quantitative analysis. Therefore, kinematic analysis is adopted as the main approach in this work. The dynamic maneuver is an interesting but challenging approach, which requires a motion model and a suitable sensory feedback mechanism. It is under investigation as well.

Figures 11 and 12 also show the challenge for a robot with low DOFs when climbing an obstacle of comparable size. The COM trajectory of the cockroach climbing the step increases smoothly (Watson *et al* 2002b). Though no force data were reported, a smooth force transition is expected. In contrast, the robot, with limited DOFs, has to perform dedicated maneuvers, first posing the body in the right configuration (S03 and S04) and then lifting the body (S05). The forces transmitted between the bottom and the top force plates in motions S03 and S04 are not for body lifting, but for preparing the right body posture. This procedure may be omitted if the robot has higher DOFs or actuating power density.

5. Conclusion

In this paper, we report on the design and implementation of an autonomous step-climbing maneuver in a RHex-style hexapod robot with a leg length of 107 mm and a standing body height of 142 mm. The robot, using its original tripod walking gait, can climb steps as high as 150 mm; by utilizing the proposed algorithm, however, it can reliably climb steps up to 250 mm high, 67% higher than the height of the robot and 2.3 times the length of its legs. The algorithm is inspired by

the observation that a cockroach changes from a tripod gait to a specific climbing maneuver in order to climb steps. Similar to the motion of the cockroach, the developed maneuver is composed of two stages: the ‘rearing stage’, inclining the body so the front is raised, thereby making it easier for the front legs to catch the top of the step, followed by the ‘rising stage’, maneuvering the COM of the body to the top of the step. The detailed quantitative work was primarily developed based on the kinematic motion of the robot, including the idea of leg-rolling motion, instantaneous center of rotation, trajectory generation, etc. Because of the limited active DOFs on the robot, the bio-inspired behavior requires a dedicated motion design. IR sensors are utilized to detect the presence of the step and the configuration of the step relative to the robot’s heading. With heading posture up to ± 40 degrees, the step-climbing maneuver is initiated, and the tilted posture can be successfully corrected. An inclinometer is utilized to detect the height of the step during climbing, in order to enable the robot to generate automatically the adequate maneuver in real time, and to climb steps 150–250 mm high. The inclinometer is also used to detect the shape of the obstacles (narrow bar, bar or step), so the robot can successfully transition from the climbing maneuver back to the normal tripod-walking gait. The performance of the algorithm was experimentally evaluated in a statistical manner by analyzing the trajectories of the robot COM and the ground reaction force. In the overall step-climbing maneuver, the RMS error between the averaged robot trajectory and the kinematic simulation is 10.1 mm, 2% of the body length. Because the empirical robot trajectories are similar to the developed kinematic-based trajectory, we can conclude that the step-climbing maneuver is basically quasi-static. Thus, although the straightforward and feasible kinematic analysis is not as realistic as dynamics, it is sufficient to yield adequate performance in this particular application.

We are in the process of developing a more advanced sensory system, such as a stereo vision system or a 3D laser scanner, together with an object recognition technique, to distinguish different types of obstacles in the robot’s locomotion path. In the meantime, we are investigating other rough terrain negotiation methods, in order to enable the robot to move autonomously over a wider range of unconstructed rough terrains.

Acknowledgments

This work is supported by National Science Council (NSC), Taiwan, under contract 97-2221-E-002-208-MY3 and 100-2628-E-002-021-MY3. The authors thank the National Instruments Taiwan Branch for their kind support of equipment and technical consulting.

References

- Bogges M J, Schroer R T, Quinn R D and Ritzmann R E 2004 Mechanized cockroach footpaths enable cockroach-like mobility *IEEE Int. Conf. on Robotics and Automation (ICRA)* (26 April–1 May 2004) vol 3 pp 2871–6
- Boxerbaum A S, Oro J and Quinn R D 2008 The latest generation Whegs robot features a passive-compliant body joint *IEEE Int. Conf. on Robotics and Automation (ICRA)* (19–23 May 2008) pp 1783–4
- Camhi J M and Johnson E N 1999 High-frequency steering maneuvers mediated by tactile cues: Antennal wall-following by the cockroach *J. Exp. Biol.* **202** 631–43
- Cham J G, Karpick J K and Cutkosky M R 2004 Stride period adaptation of a biomimetic running hexapod *Int. J. Robot. Res.* **23** 141–53
- Chou Y-C, Yu W-S, Huang K-J and Lin P-C 2011 Bio-inspired step crossing algorithm for a hexapod robot *IEEE/RSJ Int. Conf. Intelligent Robots and Systems (IROS)* pp 1493–8
- Clark Haynes G and Rizzi A A 2006 Gaits and gait transitions for legged robots *IEEE Int. Conf. on Robotics and Automation (ICRA)* (15–19 May 2006) pp 1117–22
- Cowan N J, Lee J and Full R J 2006 Task-level control of rapid wall following in the American cockroach *J. Exp. Biol.* **209** 1617–29
- Dickinson M H, Farley C T, Full R J, Koehl M A R, Kram R and Lehman S 2000 How animals move: an integrative view *Science* **288** 100–6
- Full R J and Koditschek D E 1999 Templates and anchors: neuromechanical hypotheses of legged locomotion on land *J. Exp. Biol.* **202** 3325–32
- Goldman D I, Chen T S, Dudek D M and Full R J 2006 Dynamics of rapid vertical climbing in cockroaches reveals a template *J. Exp. Biol.* **209** 2990–3000
- Harley C M, English B A and Ritzmann R E 2009 Characterization of obstacle negotiation behaviors in the cockroach, *Blaberus discoidalis* *J. Exp. Biol.* **212** 1463–76
- Jusufi A, Kawano D T, Libby T and Full R J 2010 Righting and turning in mid-air using appendage inertia: reptile tails, analytical models and bio-inspired robots *Bioinspir. Biomim.* **5** 045001
- Kalakrishnan M, Buchli J, Pastor P, Mistry M and Schaal S 2011 Learning, planning, and control for quadruped locomotion over challenging terrain *Int. J. Robot. Res.* **30** 236–58
- Kim S, Clark J E and Cutkosky M R 2006 iSprawl: design and tuning for high-speed autonomous open-loop running *Int. J. Robot. Res.* **25** 903–12
- Kohlsdorf T and Biewener A A 2006 Negotiating obstacles: running kinematics of the lizard *Sceloporus malachiticus* *J. Zool.* **270** 359–71
- Kohlsdorf T and Navas C A 2007 Evolution of jumping capacity in Tropicurinae lizards: does habitat complexity influence obstacle-crossing ability? *Biol. J. Linn. Soc.* **91** 393–402
- Lewinger W A, Harley C M, Ritzmann R E, Branicky M S and Quinn R D 2005 Insect-like antennal sensing for climbing and tunneling behavior in a biologically-inspired mobile robot *IEEE Int. Conf. on Robotics and Automation (ICRA)* (18–22 April 2005) pp 4176–81
- Lin P C, Komsuoglu H and Koditschek D E 2005 A leg configuration measurement system for full-body pose estimates in a hexapod robot *IEEE Trans. Robot.* **21** 411–22
- Lin P C, Komsuoglu H and Koditschek D E 2006 Sensor data fusion for body state estimation in a hexapod robot with dynamical gaits *IEEE Trans. Robot.* **22** 932–43
- Low K H and Chong C W 2010 Parametric study of the swimming performance of a fish robot propelled by a flexible caudal fin *Bioinspir. Biomim.* **5** 046002
- Moore E Z and Buehler M 2001 Stable stair climbing in a simple hexapod robot *4th Int. Conf. on Climbing and Walking Robots (CLAWAR)* pp 603–10
- Moore E Z, Campbell D, Grimminger F and Buehler M 2002 Reliable stair climbing in the simple hexapod ‘RHex’ *IEEE Int. Conf. on Robotics and Automation (ICRA)* pp 2222–7
- Okada J and Toh Y 2000 The role of antennal hair plates in object-guided tactile orientation of the cockroach (*Periplaneta americana*) *J. Comp. Physiol. A* **186** 849–57

- Plamondon N and Nahon M 2009 A trajectory tracking controller for an underwater hexapod vehicle *Bioinspir. Biomim.* **4** 036005
- Quinn R D, Nelson GM, Bachmann R J, Kingsley D A, Offi J T, Allen T J and Ritzmann R E 2003 Parallel complementary strategies for implementing biological principles into mobile robots *Int. J. Robot. Res.* **22** 169–86
- Saranli U, Buehler M and Koditschek D E 2001 RHex: a simple and highly mobile hexapod robot *Int. J. Robot. Res.* **20** 616–31
- Shaoping B, Low K H and Weimiao G 2000 Kinematographic experiments on leg movements and body trajectories of cockroach walking on different terrain *IEEE Int. Conf. on Robotics and Automation (ICRA) (2000)* vol 3, pp 2605–10
- Spagna J C, Goldman D I, Lin P, Koditschek D E and Full R J 2007 Distributed mechanical feedback in arthropods and robots simplifies control of rapid running on challenging terrain *Bioinspir. Biomim.* **2** 9–18
- Sponberg S and Full R J 2008 Neuromechanical response of musculo-skeletal structures in cockroaches during rapid running on rough terrain *J. Exp. Biol.* **211** 433–46
- Watson J T, Ritzmann R E and Pollack A J 2002a Control of climbing behavior in the cockroach, *Blaberus discoidalis*: II. Motor activities associated with joint movement *J. Comp. Physiol. A* **188** 55–69
- Watson J T, Ritzmann R E, Zill S N and Pollack A J 2002b Control of obstacle climbing in the cockroach, *Blaberus discoidalis*: I. Kinematics *J. Comp. Physiol. A* **188** 39–53
- Weingarten J D, Groff R E and Koditschek D E A 2004 Framework for the coordination of legged robot gaits *IEEE Int. Conf. on Robotics, Automation and Mechatronics (RAM)* pp 679–86
- Zucker M, Ratliff N, Stolle M, Chestnutt J, Agnell J A, Atkeson C G and Kuffner J 2011 Optimization and learning for rough terrain legged locomotion *Int. J. Robot. Res.* **30** 175–91